(3+1)-dimensional optical soliton dragging logic

Robert McLeod, Kelvin Wagner, and Steve Blair
*Optoelectronic Computing Systems Center, University of Colorado, Boulder, Colorado 80309-0425**
(Received 23 February 1995; revised manuscript received 4 May 1995)

A review of the varieties of optical solitons and their possible interactions, combined with the requirements for a robust digital logic gate motivate the use of (3+1)-dimensional optical solitons (light bullets) as information carriers and soliton dragging gates as switches. Soliton dragging is the asymmetric interaction between two initially overlapping, orthogonally polarized solitons propagating at different angles so that a weak signal soliton can drag a strong pump out of a spatial aperture, thereby implementing a phase-insensitive, high-contrast, logical switch with gain. Light bullets may be an ideal choice for use in these soliton dragging gates but are unstable in Kerr media, but stable (for sufficient pulse energy) in materials with physically reasonable saturating or negative $n_4 I^2$ nonlinearities. An efficient technique for the propagation of spherically symmetric (3+1)-dimensional field envelopes is developed and used to verify the theoretical stability predictions. A split-step numerical algorithm that models the propagation and phase-independent interaction of arbitrary (3+1)-dimensional, vector e.m. fields in anisotropic media with up to sixth-order tensor nonlinearities is developed and used to demonstrate the features of the gates. NOT and single-stage, two- and four-input NOR light-bullet dragging logic gates are simulated and their performance over a range of operating parameters is presented. It is shown that, with material parameters in the range of those currently available from highly nonlinear organic crystals, high-contrast, all-optical, soliton logic gates with a clock rate greater than 1 THz, latency of a few picoseconds, and switching energy of 25 pJ may be possible.

PACS number(s): 42.50.Rh, 42.50.Ne, 42.65.−k

I. INTRODUCTION

Optical solitons may soon be the primary carriers for long- and short-distance information transmission because, unlike pulses in a linear dispersive fiber, solitons are self-confined, propagating long distances without changing shape [1]. Also unlike light in linear media, solitons can interact; while this is a source of timing jitter to be avoided in a communication system, this interaction can form the basis of an all-optical switch [2]. Because solitons exhibit a critical threshold energy—below which they spread and above which they become self-contained—they are also natural carriers of *binary* information. Thus solitons and soliton interactions are well matched to the potential application of all-optical, digital computing.

As early as the 1960s, it was recognized that Kerr self-focusing of beams with Gaussian profiles could create one-dimensional self-guided waves [3–5]. These one-dimensional spatial solitons in slab waveguides are created by the balance of nonlinear self-focusing and diffraction. The properties of these solitons are determined from the nonlinear Schrödinger equation (NLSE) which describes the propagation of the slowly varying, paraxial envelope of the electric field. The equation always contains one propagation dimension and between one and three transverse dimensions which describe solitons with one, two, or three dimensions of self-induced confinement [often referred to as (1+1)-, (2+1)-, or (3+1)-dimensional propagation]. The equation treats time and space dimensions identically, yielding the well-known result [6] that the spatial dynamics of one-dimensional spatial solitons are in fact identical to the temporal dynamics of one-dimensional temporal solitons; one simply needs to replace the spatial quantities of nonlinear self-focusing, diffraction, and spatial frequency (angle) with their temporal analogs of nonlinear pulse compression, anomalous group-velocity dispersion, and temporal frequency (color). Thus, by analogy with one-dimensional spatial solitons, one-dimensional temporal solitons in optical fiber are created by the balance of nonlinear pulse compression and anomalous group-velocity dispersion (AGVD).

In both spatial and temporal one-dimensional solitons, the pulse is either localized in the remaining dimensions by static dielectric guiding (e.g., the fiber core or a slab waveguide) or is unbounded and infinite (e.g., the cw beam of the spatial soliton). Within the limits in which the NLSE is derived (such as the effective-index approximation) the propagation equation is independent of whether any of these dimensions is linearly guided or unbounded — the only modification is that the dispersion relation for the optical wave vector must include the correct guided-wave and/or bulk material dispersion terms. In the case of linearly guided waves, the material normal group-velocity dispersion (NGVD) can be dominated by guided-wave anomalous group-velocity dispersion, which is required for bright temporal solitons. Both temporal and spatial one-dimensional (1D) solitons have been extensively analyzed [6] and demonstrated experimentally [1,7].

Two-dimensional solitons can be nonlinearly confined in either (a) two transverse space dimensions or (b) one space and one time dimension. Two-dimensional steady-state spatial filaments are formed in bulk media by the balance of radially symmetric nonlinear self-focusing and diffraction. Analogously, 2D spatiotemporal solitons are formed in slab waveguides by the simultaneous effects of spatial self-focusing and temporal pulse compression which are counter-

*Phone: (303) 492-4716; FAX: (303) 492-3674.

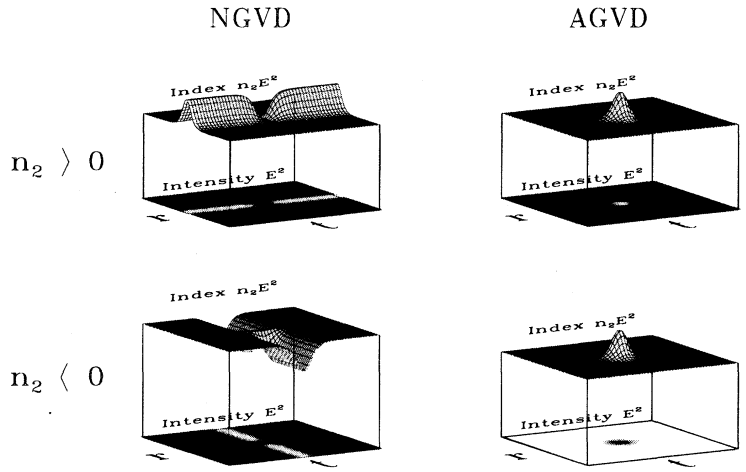

FIG. 1. Possible types of bright and dark solitons for two- and three-dimensional space-time waves showing the light intensity pattern (bottom) and associated nonlinear index distribution (top). The variable t represents the temporal or propagation axis, while r represents the transverse Cartesian spatial coordinate in the case of two-dimensional solitons or the transverse radial spatial coordinate in the case of three-dimensional solitons. In this case, the figure illustrates a slice through the radially symmetric intensity profile.

acted by diffraction and guided-wave anomalous group-velocity dispersion, respectively. Without a modification of the Kerr-law nonlinearity, both types of 2D solitons are inherently unstable and break up into multiple filaments [8] or approach a critical focus at which point the approximations of the NLSE break down and higher-order dispersion, diffraction, and nonlinearities must be included [9]. Strictly speaking, these "2D solitons" are solitary waves, not solitons, because the nonlinear Schrödinger equation which describes their propagation is not an integrable system in any but the one-dimensional case. We will follow the usual convention, however, and use the loose terminology of solitons.

The existence of three-dimensional optical solitons, which feature simultaneous radially symmetric 2D spatial self-focusing and temporal pulse compression, has recently been suggested [10,11]. Unlike one- or two-dimensional solitons, these (3+1)-dimensional optical solitons ("light bullets") are completely localized and are confined purely by nonlinear effects; they do not require any static dielectric waveguide, but as a result cannot take advantage of the interplay of dielectric confinement and material dispersion to yield a region of anomalous GVD. Like lower-dimensional solitons, the spatial profile of a light bullet is created by the balance of Kerr self-focusing and diffraction, while its temporal pulse shape is determined by the balance of Kerr pulse compression and group-velocity dispersion. Like 2D solitons, they are also inherently unstable to propagation in Kerr media [12,13].

Analogs of all of these solitons exist in negative Kerr, or self-defocusing, nonlinear media. One- and two-dimensional spatial dark solitons propagate as nondiffracting dark holes in materials with $n_2<0$. One-dimensional temporal solitons in a continuous beam are moving dark pulses which do not disperse if the nonlinear index and the group-velocity dispersion constant ($\partial^2 k/\partial\omega^2$) have the same sign. Finally, two- and three-dimensional spatiotemporal solitons can be bright in one direction and simultaneously dark in another, as illustrated in Fig. 1. While dark solitons can have continuous phase, they can also be "vortex solitons" which instead contain a linear or spiral phase discontinuity at the location of zero intensity. This variety of forms in the case of spatiotemporal solitons arises from the fact that the temporal dispersion can be either positive or negative. In contrast, the spatial diffraction is always positive (except in rare cases such as near an optical axis in a biaxial anisotropic crystal).

These mixed bright-dark solitons are not likely to be stable (although we know of no such analysis in the literature) although it is possible that modified nonlinearities (e.g., saturation) and optical phase discontinuities (e.g., vortex solitons) could restore stability. To be stable, the dark soliton profile (vs r and t) must itself be stable to propagation. Simultaneously, the bright background soliton (which is a radially confined beam in the $n_2>0$, NGVD case and a temporally confined plane wave in the $n_2<0$, AGVD case) must also be robust to both perturbations in the confined direction as well as modulation instabilities along its unbounded direction. This second problem has been analyzed extensively [14,15]. The stability of dark optical bullets — the three-dimensional version of the $n_2<0$, AGVD soliton — has recently been shown using variational techniques [16].

As illustrated in the figure, in AGVD regimes, the decrease of intensity in the dark region, when multiplied by the negative Kerr coefficient, results in an increase in the local refractive index. Thus these dark solitons can interact in the same manners that bright solitons do [17].

The properties of all of these pulses — one-, two-, or three-dimensional and bright or dark — are derived from the appropriate nonlinear Schrödinger equation by assuming a solitary wave solution and forcing it to fit the boundary conditions. To be seen in the laboratory, however, these solutions must also be robust to perturbations. Of the bright solitons, only one-dimensional temporal and spatial pulses are inherently robust to propagation — higher-dimensional solitary waves, while eigen-solutions of the NLSE, suffer from a variety of instabilities including breakup into multiple waves [8], instability to modulation in an unguided dimension [14], and exponential growth of azimuthal perturbations [18]. These dynamics are separate from the phenomenon of critical collapse, in which incident fields with considerably more energy than the fundamental soliton self-focus to an infinitesimal point.

Both propagation instabilities and critical collapse can be counteracted by considering non-Kerr media. For example, in reality the nonlinear index cannot actually increase without bound but must instead saturate at some level; at even higher intensities it will suffer permanent damage. By in-

cluding a nondamaging saturating nonlinearity in the nonlinear Schrödinger equation, stable two-dimensional solitons have been predicted [19]. This is physically reasonable since a strongly saturated nonlinear material will resemble a step-index waveguide [20], which is well known to support stable guided waves (e.g., fibers). Analogously for three dimensions, the stability and even bistability of light bullets have been shown numerically using simple and multilevel saturating nonlinear index variations [21]. Numerical studies have also shown that saturation causes one-dimensional solitons to be more stable and to settle more quickly into steady profiles when launched from arbitrary initial conditions [22]. These stabilized soliton waves are system attractors: arbitrary pulses not too far from the soliton profile will form into solitons, and lower-dimensional envelopes will break up into sets of higher-dimensional solitons. For example, a cw Gaussian beam with a small temporal modulation propagating in a saturating nonlinear material with AGVD will spontaneously divide into a chain of light bullets [23].

While saturation and similar effects are the stabilization techniques of interest in this study, it is worth mentioning that more exotic methods have also received attention. For instance, a second optical pulse of a different color can be used to modify the index profile seen by the soliton pulse [11]. More directly, the linear index of the medium can be modulated to produce a static transverse index profile [24], although this tends to blur the distinction between self-guided and linearly guided waves. Finally, vortex solitons are dark solitons in which a topological constraint — a linear phase discontinuity of $(2n+1)\pi$ in one dimension or a phase spiral of $2n\pi$ in two dimensions — forces there to be a region of zero intensity, helping to stabilize the dark soliton [25].

Unlike optical pulses in linear media, these stabilized one-, two-, or three-dimensional solitons can interact through their nonlinearly induced index change. In the following sections, we summarize the varieties of these interactions and compare their features to the requirements for all-optical digital logic in order to motivate the use of light bullets as digital-information carriers and the basis of a logic system. Following that, we derive the properties of light bullets from the e.m. wave equation and show that they can be stabilized in non-Kerr media of two common types. In the final two sections, we develop a split-step numerical technique for vector e.m. waves in anisotropic materials with tensor nonlinearities and use this technique to numerically investigate the properties of light-bullet dragging logic gates.

II. SOLITON INTERACTIONS

As discussed above, there are a wide variety of optical solitons that could be used as information carriers. There are are also a variety of ways in which two solitons can be made to interact in order to form a switch or logic gate. These different soliton interactions have very different properties which will in turn strongly influence the operation of the logic circuit. In order to motivate our choice of the dragging interaction, in this section we briefly compare the ways in which a pair of one-, two-, or three-dimensional solitons can interact.

The properties of these interactions are determined solely by the initial conditions of the two solitons. These initial conditions are (1) the polarizations and possibly relative phase of the two pulses and (2) the positions and relative transverse velocity of the two waves. The first condition, the electric polarizations of the two e.m. waves, will strongly influence the behavior of the interaction. If the two fields are copolarized, they will produce an intensity interference pattern which is explicitly dependent on their relative phase. If the two bright solitons are in phase, this pattern will have a constructive maximum between the two solitons which will increase the nonlinear optical index (through the positive Kerr nonlinearity, $n=n_0+n_2|E|^2$) causing an initially attractive force. Conversely, if the solitons are π out of phase, the destructive interference null will create a minimum in the index between the two waves which will tend to push the two pulses apart.

To avoid this dependence on the optical phase, the two solitons can be oriented in orthogonal optical polarizations. The physics of the Kerr interaction must now be described by the fourth-order $\chi^{(3)}$ tensor, rather than the scalar n_2 model which is only sufficient for single polarizations. In isotropic materials, the form of this tensor may still create phase-dependent terms in the interaction due to periodic traveling-wave susceptibility gratings, but proper choice of the orthogonal polarization basis can remove these terms [26]. Alternately, when the material is birefringent, either because the medium is anisotropic or through form birefringence (e.g., a waveguide), the difference in the propagation constants of the two polarizations will phase mismatch these phase-dependent terms if the interaction is sufficiently long (this topic is more fully discussed in Sec. VI, below). In these cases — two orthogonally polarized solitons interacting in a phase-independent fashion — the forces between the two solitons are attractive only, via the cross-phase modulation of the two waves.

Thus the polarizations (and in some cases phase) of the two solitons determine the direction of the force between them. Knowing this, one can then examine the second important initial condition, the geometry, to predict the properties of the interaction. This geometry consists of the relative transverse spacing, transverse velocity, and powers of the two solitons. These are all continuous variables, but numerical and experimental studies have shown that distinctly different behavior occurs for different ranges of the initial geometrical parameters. These different behaviors can be used to classify this wide variety of interactions into a relatively small number with noticeably different features.

Figure 2 schematically illustrates these unique initial geometries in one-, two-, and three-dimensional two-soliton interactions. As discussed in the Introduction, within the approximations made in deriving the NLSE, spatial and temporal solitons have the same dynamics. Thus the arrows in Fig. 2, indicating an initial relative transverse velocity, can be viewed as either a relative direction of propagation for spatial soliton interactions or a relative group-velocity difference in the case of temporal soliton interactions. Several of the interaction geometries can be immediately dismissed as not useful for switching. Geometries in which the solitons are separated and initially traveling away from one another will exert minimal nonlinear forces on one another which will result in essentially *no switching*. Conversely, if the two

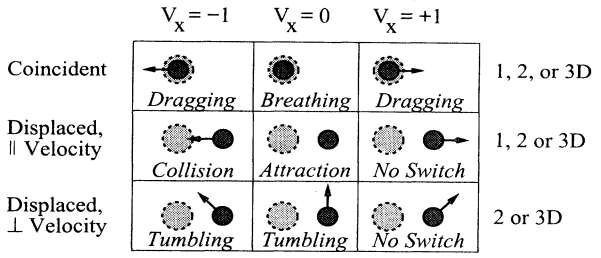

FIG. 2. Possible two-soliton interaction geometries for positive (attractive) cross-phase modulation. The two one-, two-, or three-dimensional solitons are represented by circles which can be coincident or displaced in a transverse temporal or spatial dimension. The arrows indicate an initial transverse velocity of one soliton relative to the other, which can be parallel to the displacement, or have a component which is perpendicular. Because the bottom row utilizes transverse velocity components in two dimensions, one-dimensional solitons cannot interact in these manners. The outcome of these initial conditions will depend on the nature of the nonlinear interaction (such as its phase dependence) as well as the relative powers of the two solitons.

solitons are separated and initially traveling towards one another, but with a second component of velocity orthogonal to the line of separation, an attractive nonlinear force (via either orthogonal polarizations or in-phase copolarized pulses) will result in spiraling or *tumbling* of the two solitons [27,28]. Although it might be possible to construct a switch or logic gate from this interaction, the complexities of the motion would make the implementation difficult. This leaves the four simple one-dimensional interactions in the upper-left portion of Fig. 2 as candidates for a soliton-soliton switch (these are also illustrated for the case of spatially interacting light bullets in Fig. 3).

In soliton *attraction* and *repulsion* interactions, the two solitons are initially separated and propagate collinearly — with the same frequency and thus velocity if temporally confined or at the same angle if spatially confined. If the two solitons are copolarized and π out of phase, they repel. This repulsive force can form the basis of a switch or logic gate. In a spatial soliton repulsion gate [29], for example, two one-dimensional spatial solitons are launched in the same direction, separated by a few beam widths but π out of phase. The repulsive force on the two solitons creates a change in their angles of propagation. After a sufficient distance, the presence or absence of one soliton can be detected by the position of the other beam, thus forming the basis for a logical decision. If the solitons are in phase or cross polarized, the beams attract and can form a trapped pair, which could also be used as a logic device. Soliton interactions of these types have been observed experimentally [30].

If the two solitons are initially separated but directed towards one another, they will *collide* at some point within the nonlinear medium. Copolarized spatial solitons can be made to collide by launching them with different angles, while temporal solitons can collide if given different colors and thus different group velocities. In anisotropic crystals, anisotropic walk off can be used to bring cross-polarized solitons together in space. Analogously, cross-polarized temporal solitons of the same color will collide in birefringent fibers.

This collision interaction is based on the fact that, in one

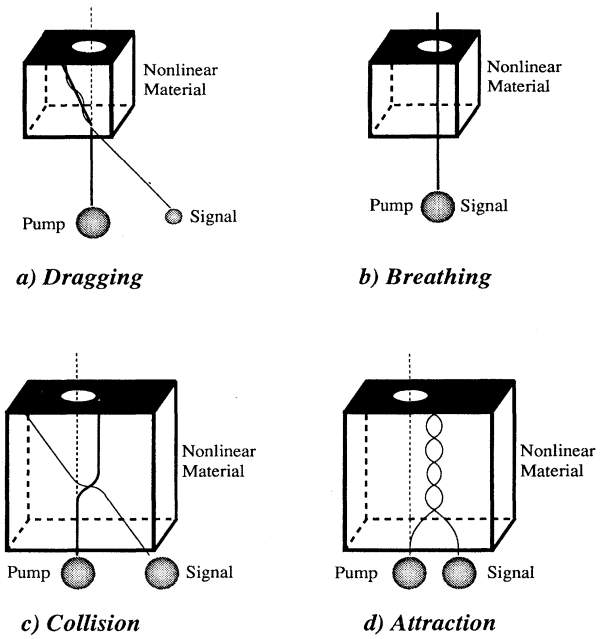

FIG. 3. Comparison of dragging, breathing, collision, and attraction light-bullet logic gates for a purely attractive ($n_2>0$), phase-insensitive interaction. The logical decision is implemented by the aperture in the output plane, which passes (output equals one) or blocks and dissipates (output equals zero) the pump soliton.

dimension, copolarized solitons (and in one case, cross-polarized solitons) are described by an integrable system of equations and thus two colliding solitons that are initially well separated must emerge from the collision unchanged except for a small positional shift (for spatial soliton collision) or a temporal shift (in the case of temporal soliton collision). In particular, the initial angle of spatial propagation or velocity of temporal propagation will be restored for each soliton. In nonintegrable systems — 1D cross-polarized waves with the ratio of cross- to self-phase modulation not equal to one and all 2D and 3D solitons — this return to the initial propagation direction is not perfect, but is nearly so, at least for large-angle collisions. Since the final velocity equals the initial, increased gain cannot be produced by an increase in interaction distance and thus collision interactions cannot produce large gain. It has recently been shown that small-angle collision of vector solitons can result in gain [31]. However, the behavior of the collision in this case depends sensitively on the incidence angle; as discussed in the next section, such a sensitivity will make it difficult to use this interaction in any large-scale optical circuit.

The collision interaction has been suggested as a mechanism for a photonic switch [32], has been demonstrated experimentally using dark spatial solitons [33], and has been studied as the basis of a logic family [17]. A number of authors have examined the possibility of guiding lower-intensity pulses in the dielectric guides induced by colliding spatial solitons [34,35]; while this phenomenon could be used for a photonic circuit switch, it is not applicable to logic interactions.

If the two solitons are both coincident and collinear, *breathing* soliton modes will be formed by the interaction of

the two cross-polarized waves [27]. In the literature, these have been referred to as new forms of vector solitons, however, they can also be viewed simply as the interaction between two cross-polarized waves. This interaction could be used as a switch by using one soliton to influence the breathing period of the other, which would efficiently pass through an aperture only if a narrow waist of the breathing mode occurred at that point. In the "off" state the soliton would encounter the aperture while much broader, consequently much less energy would be transmitted. This would be a low-contrast device and has not been examined in the literature.

The final type of soliton interaction is created when the two solitons are initially coincident but directed at different spatial angles or temporal frequencies. This *dragging* interaction (sometimes referred to as "trapping" [2]) can be viewed as a modification of the collision interaction except that the approach to collision is in a linear medium where no interaction takes place; the nonlinear effects occur only from the collision point onwards. With temporal solitons, for example, this breaks the symmetry of the collision by which a soliton's frequency is changed as the solitons approach and then is reset as they separate. If the initial frequency difference and energy ratio of the two solitons is not too great and the force between them is attractive, the solitons can form a bound, stable pair which propagates at approximately the mean velocity of the individual solitons, weighted by their individual momenta. This asymmetric "temporal soliton dragging" interaction has been proposed as an all-optical logic gate and demonstrated in fibers [36] by measuring the time shift due to the accumulated change of velocity of the solitons after collision. It has also been observed using copolarized 1D spatial solitons in CS_2 liquid [37], but the performance as a switch with gain was not investigated.

If the initial transverse velocity or energy difference is so large that the two solitons cannot form a bound state, the asymmetry of the interaction (in comparison to a symmetric collision at large angle) will still cause the two solitons to emerge with a permanent velocity shift. This "deflection" operation is thus very similar to the trapping geometry except that the total velocity shift is reduced [38].

The dragging interaction has a number of advantages over attraction-repulsion and symmetric collision devices. First, since the solitons emerge from the initial collision point with a permanent velocity shift, it is possible to create much larger time or space shifts than the symmetric collision induces. Unlike any of the previously described interactions, it is also easy to switch an intense pump soliton with a weaker signal soliton, resulting in logical signal restoration (gain) — an essential feature for any cascadable logic device. This combination of high contrast and high gain is often difficult to obtain in nonlinear switching devices that utilize diffracting beams due to the inherent tradeoff of beam size (intensity) and confocal distance (interaction length). Solitons overcome this tradeoff and make possible tightly confined beams that can interact over long distances. The dragging interaction takes advantage of this feature of solitons by forming a bound soliton pair which interact over the entire length of the switch. Nonlinear devices that use a waveguide to confine the optical power have the same advantage, but they have the disadvantage that they cannot be operated in parallel in a uniform volume of material.

By only using the undragged pump in later stages and blocking any dragged solitons, the dragging operation also provides true three-terminal operation with input-output isolation. Finally, by using pump and signal temporal solitons in different optical polarizations that interact only through the intensity-dependent cross-phase modulation, the logic gate becomes insensitive to phase [2], unlike the inherently phase-dependent repulsion interaction.

Recently [39,22], it was noted that the phase-insensitive, orthogonally polarized soliton dragging interaction, developed and investigated for temporal solitons, can be applied to spatial solitons as well. A distinct advantage of the spatial soliton dragging gate is that the logical decision is made by an aperture in the output plane which passes or blocks the pump soliton—a considerably easier decision than ultrafast temporal coincidence detection [38] or narrow-band spectral filtering [2]. Numerical studies of this logic gate showed that it should not be difficult to construct a phase-insensitive spatial soliton dragging gate with high contrast and gain of 4 in a propagation distance of only ten confocal lengths.

III. REQUIREMENTS FOR DIGITAL OPTICAL LOGIC

The theoretical, experimental, and numerical studies discussed above reveal the wealth of physical interactions that can be used to construct soliton logic gates. In many of these studies, the motivation for the work is said to be the construction of a digital logic gate. It is well known among designers of electronic digital logic, however, that the simple ability to switch one signal by another is not sufficient to construct large-scale logic circuits. This is illustrated by the fact that electronic logic is so prevalent and that, despite a significant research effort, optical logic is not. By examining the features of electronic circuits that have made them such a huge success, one can list the essential properties that a proposed optical logic family must possess if it is to make it out of the laboratory [40]. The most important of these follow.

Logical completeness. Obviously, to be generally useful, the individual logic gates must be able to be interconnected to implement any possible logical function. In their simplest form, most soliton logic gates are inverters — the pump is passed (output equals one) only if the signal is not present to deflect it (input equals zero). The ability to construct a NOT gate is important because all complete logic families are able to perform this operation. NOR gates form such a logically complete set and can be constructed from soliton interactions by a cascade in which multiple, successive signal solitons can interact with a single common pump. In other words, the pump soliton is passed through a series of gates; the presence of a signal in any one of which will deflect the pump and cause it to be blocked, producing the correct low output of a NOR.

Three-terminal device. These logically complete gates can reliably be combined into circuits only if they are true three-terminal devices. That is, photons enter the gate (terminal one) and exit the output (terminal two) controlled by the input signal (terminal three). The input must be isolated from the output so that processing proceeds in only one direction, and the output must be standardized to one of two binary levels, independent of all variations of the input signal ex-

cept its digital value. This can be accomplished in soliton logic gates by supplying a pump soliton from the power-supply laser at each gate, which is passed on as the output only if no signal soliton is present and is blocked otherwise. Thus the timing, position, direction of propagation, energy, polarization, phase, and wavelength of the output soliton are restored by the power supply at each gate. In addition, the output of one gate is used as the input of a subsequent gate where these signal photons drag the pump and are then discarded. Thus, from stage to stage, logical information is propagated, but physical photons are not.

Thresholding. In a digital (as opposed to analog) circuit, signals entering a gate must be classified into their discrete digital values based on the thresholding of the analog levels. The nature of soliton propagation provides a natural thresholding operation — a pulse can only propagate as a soliton if it contains at least the soliton critical energy, otherwise it rapidly diffracts and/or disperses. This digital nature of soliton propagation makes solitons natural carriers of binary information.

Cascadability. A number of optical logic devices have been proposed which change the nature of the information carrier in the gate such that the output of one gate cannot be used as the input to another. A common example is a change in the color of the light. From the viewpoint of a circuit designer, devices of this type are little more than intellectual curiosities since they cannot be used in combination. Temporal soliton logic gates, which use different color pulses to create an initial velocity difference, fall in this category. These devices could be cascaded by alternating them in layers in which the color of the light switches back and forth; however, it is usually the case that only one of the two types of required devices is easily constructed. The remainder of soliton logic gates, in general, do not change the color of the light but may instead, if they employ orthogonally polarized solitons, change the polarization at each stage. In this case, it is a simple matter to alternate the polarizations of signal and pump at each level. Thus most soliton logic gates are cascadable but most do suffer from a more common limit to cascadability which is a lack of gain.

Gain. Gain is the ability of the gate to drive outputs that are more energetic than the inputs. If a logic device has no gain, the output levels must always be less than the inputs and eventually the output of one gate will have insufficient energy to switch the next. Surface reflection and diffraction losses in optical systems make this particularly significant when designing digital optical circuits. Gain is also essential since the output of any gate is inevitably required to drive the inputs of more than one subsequent gate (fan out). Only soliton dragging gates can easily achieve large gain and thus be truly cascadable. Although these gates are passive, with no electrical pump or inverted medium, they can still achieve gain because a small signal can drag a larger pump.

Parallelism. One of the major achievements of modern electronics was the transition from single, bulk transistors to densely packed very large-scale integrated (VLSI) circuits in which thousands of gates are operating simultaneously in a small area. Similarly, any optical logic technology which cannot be fabricated to operate many gates with high density in a small area will not be competitive. Different soliton logic operations allow varying degrees of dense parallel operation. Temporal soliton logic gates in fibers can only be parallelized by complete duplication of the hardware, which is expensive and does not achieve high density. One-dimensional spatial soliton gates in waveguides can be operated in parallel by running many gates in the same wide slab waveguide, but can only be extended to two dimensions of parallelism by stacking these waveguides. To create extremely fast machines with many parallel channels, two or even three dimensions of inherent parallelism are desirable. In general, the number of dimensions in which a soliton logic device can be directly parallelized is equal to the dimensionality of the soliton itself since in the remaining dimensions the pulse is either infinite or confined by a static waveguide. Thus logic gates based on 1D solitons can be operated in parallel in one dimension, while devices based on 3D light bullets could have three dimensions of parallel operation.

Speed. High-speed operation is arguably the single most important feature of a device technology and is the primary reason for investigating optical soliton logic. It is shown in Sec. VII that light-bullet dragging logic can operate at greater than THz rates, which is far enough beyond current electronics technology to justify its exploration. Implemented in currently available nonlinear materials, light-bullet gates promise a switching energy of about 25 pJ, considerably higher than VLSI technology. However, an examination of the scaling law for these more conventional technologies reveals that power requirements increase supralinearly with speed, and reach an eventual upper speed limit. That is, higher-speed operation requires increasing switching energy. Thus the larger switching energy of soliton logic at its greatly increased speed actually compares well with VLSI and similar technologies.

Pipelining. The effective throughput of an electronic circuit can be increased by building the circuit such that multiple calculations can happen as a cascade within the circuit, reducing the effective time per operation from the latency of the circuit, which is the sum of all gate delays, to a latency of only a few gates. Pulsed optical soliton gates can go beyond this circuit-level pipelining and cascade multiple calculations within a single logic gate, reducing the time per calculation to much less than the latency of a single gate. This is accomplished by launching trains of solitons which interact while propagating through the gate as a traveling wave. While the gate can be arbitrarily long, it is only necessary to separate the adjacent logical signals far enough so that they do not interact. While gate-level pipelining can overcome the long latency of a gate, low latency is still important in circuits where feedback is employed. Spatial soliton gates can have latencies in the 10 ps regime, while temporal soliton gates in fibers are very long and have latencies measured in hundreds of ns. On the other hand, temporal solitons are more easily pipelined than steady-state spatial solitons. Spatiotemporal solitons (which could be either two or three dimensional) can enjoy the best of both worlds by using low-latency spatial switching with tightly packed pipelining in the temporal dimension.

Fan in. Logically complete, multiple-input NOR gates can be constructed from any of the inverting soliton interactions by cascading the pump through a succession of gates, one gate per NOR input. To interact multiple logical inputs in a single stage without strong phase sensitivity requires more

than one dimension in which to interact, thus only two- and three-dimensional solitons can support multiple single-stage fan in. Conceivably, a soliton logic gate could switch simultaneously in one space and one time dimension, but gates which instead switch in two space dimensions are much simpler to operate. This favors 2D spatial filament and 3D light-bullet solitons.

Phase insensitivity. A requirement unique to optical logic design is that the operation of the gate must be independent of the phases of its optical inputs. Otherwise, the circuit will not be robust in a large system which will expand and contract due to heat, vibration, and production tolerances. Soliton repulsion gates cannot be phase insensitive (in a positive n_2 material), while collision, attraction, and dragging gates can be made phase insensitive by using orthogonal polarizations.

Low power consumption. Realistic logic circuits contain many individual logic gates, each of which must dissipate a very small amount of energy, both to reduce the power requirement on the source laser and to limit the heat generation in the circuit. Solitons which are fully confined, either by a combination of linear and nonlinear effects (e.g., temporal solitons in fibers) or completely by nonlinear effects (e.g., light bullets) can be energy efficient. In contrast, all one-dimensional spatial soliton and two-dimensional spatial filament devices inherently consume large energy because of their quasi-cw nature. Dark soliton devices, which require a bright background, also must dissipate large amounts of power.

Decreasing the energy in the soliton reduces the heat generated when this soliton is dissipated in a logical interaction. The heat generation can be further reduced by "optical cooling" in which the solitons, after interaction, are directed outside the volume of the circuit and dissipated remotely. Optical geometries which implement this cooling technique can be constructed for spatial soliton switches.

Ease of implementation. Although not a formal requirement, any proposed logic technology that cannot be easily fabricated will be at a disadvantage. Temporal soliton gates in a fiber that make logical decisions based on ultrafast coincidence detection are more difficult to implement than spatial soliton gates in which the decision is made by a simple aperture. A narrow-band optical filter can also be used to detect the frequency shift induced in the pump soliton by the temporal dragging interaction, but this introduces a loss (even at band center) which must be overcome by increased gain and is still a significantly more complex and costly device than a simple pinhole.

By comparing the varieties of optical solitons and the manners in which they can interact to the requirements for logic, above, we find that only a very few combinations of solitons and interactions are actually candidates for large-scale digital optical logic. First, to minimize energy dissipation, the soliton must be fully confined in 3D, restricting the possible solitons to 1D temporal solitons in fibers, 2D spatiotemporal solitons in slab waveguides, or 3D light bullets in bulk media. Second, to eliminate phase sensitivity, the two solitons must be in orthogonal polarizations. And finally, to achieve significant gain and to be deeply cascadable, the dragging interaction geometry must be employed.

Orthogonally polarized soliton dragging gates of 1D temporal solitons in fibers have been the subject of a number of theoretical and experimental studies [41,2]. To our knowledge, there have been no studies of interactions with 2D spatiotemporal solitons. In this study, we shall concentrate on the final choice, which is the interaction of orthogonally polarized 3D light bullets in a soliton dragging geometry.

This type of logic gate can have large gain and is three terminal, cascadable, and phase insensitive. They can be densely parallelized and pipelined, will support single-stage fan in, can be operated in the simple spatial switching geometries, and are fully localized carriers of energy. The varieties of light-bullet logic gates are illustrated in Fig. 3. Light-bullet dragging logic gates are high-speed, all-optical devices with the properties required for application to complex digital optical computing circuits.

Two-dimensional spatiotemporal solitons in a slab waveguide exhibit all of the same advantages except that they have only one dimension available for spatial interaction and thus cannot support single-stage logical fan in or three-dimensional parallelism. Fabrication issues may be simpler for these devices, however, and since the majority of the results derived in the remainder of this paper apply to 2D space-time solitons with only minor modifications, these solitons may provide the first practical proof-of-principle test bed.

Returning to the light bullet dragging gates, we must first examine the light bullets themselves. Kolokolov predicted that three-dimensional solitons in a Kerr medium would be unstable to propagation [12], which we confirm with numerical propagation in the next section. It is well known, however, that a modification of the Kerr nonlinearity can act to stabilize two-dimensional spatial solitons [18] and this has been predicted to be true for three-dimensional solitons as well [12]. Therefore, in the following section, we demonstrate the robustness of light bullets under two physically reasonable nonlinearities, those being saturation and the inclusion of higher-order ($\chi^{(5)}$) nonlinear interactions. To verify these predictions, we present a highly efficient beam-propagation technique for spherically symmetric fields.

We then describe how these stable and robust light bullets can be used to form ultrafast, efficient, digital optical logic devices with gain. In order to simulate this gate, we develop a beam-propagation algorithm for the phase-independent interactions of vector fields in anisotropic materials with up to sixth-order tensor nonlinearities. This simulation technique is used to demonstrate light-bullet dragging logic gates which have pJ switching energies, large gain, phase insensitivity, and subpicosecond switching times.

IV. LIGHT BULLETS IN KERR MEDIA

The existence and form of light bullets can be derived from the scalar electromagnetic wave equation [Eq. (1)] [10]. This equation does not include anisotropy or polarization effects (although these are introduced in Sec. VI) and assumes that the nonlinear index variation is small so that the nonlinear contribution to $\nabla(\nabla \cdot E)$ can be neglected. Because of the assumed scalar nature of the electric field, the third-order (Kerr) term in the nonlinear susceptibility ($\epsilon_{NL} = \chi^{(3)}|E|^2$) can be written as a purely scalar, rather than fourth-order tensor, equation. Although thus simplified, the

resulting wave equation is sufficient to describe a single three-dimensional paraxial soliton of a fixed optical polarization in an isotropic Kerr medium.

We begin with the three-dimensional wave equation in Cartesian coordinates for a single optical polarization, E:

$$\nabla^2_{xyz}E-\frac{1}{c^2}\frac{\partial^2 \epsilon * E}{\partial t^2}=0, \tag{1}$$

where c is the vacuum speed of light, * represent the temporal convolution operation, and ϵ is the impulse response of the relative permittivity. In the frequency domain, the convolution of the permittivity impulse response with the electric field can be represented as a product of their Fourier spectra. For this analysis we assume that this permittivity can be separated into frequency-dependent (dispersive) linear and instantaneous (nondispersive) nonlinear parts.

$$\begin{aligned}\epsilon&=\epsilon_L(\omega)+\epsilon_{NL}(E)\\&=\epsilon_L+(\omega-\omega_0)\frac{\partial \epsilon_L}{\partial \omega}\bigg|_{\omega_0}+\tfrac{1}{2}(\omega-\omega_0)^2\frac{\partial^2 \epsilon_L}{\partial \omega^2}\bigg|_{\omega_0}+\chi^{(3)}|E|^2,\end{aligned} \tag{2}$$

where $\epsilon_L(\omega)$ has been Taylor expanded to second order in frequency and $\epsilon_{NL}(E)$ has been expanded to second order in electric field. It is assumed that nonlinearities with linear dependence on the electric field are zero due to symmetry or are phase mismatched, so they will be neglected. The optical index $n=\sqrt{\epsilon}$ can be written to first order as

$$\begin{aligned}n=n_0+\frac{1}{2n_0}(\omega-\omega_0)\frac{\partial \epsilon_L}{\partial \omega}\bigg|_{\omega_0}+\frac{1}{4n_0}(\omega-\omega_0)^2\frac{\partial^2 \epsilon_L}{\partial \omega^2}\bigg|_{\omega_0}\\+n_2|E|^2,\end{aligned} \tag{3}$$

where the linear index $n_0=\sqrt{\epsilon_L}$ and the commonly tabulated Kerr nonlinear coefficient is $n_2=\chi^{(3)}/(2n_0)$ and has units of inverse electric field squared.

The definition for ϵ [Eq. (2)] contains most of the important physics for this situation. The first term (ϵ_L) is a linear isotropic instantaneous background dielectric constant. Next are the first two terms in the Taylor expansion of the dielectric variation with frequency. The linear term, involving $\partial\epsilon_L/\partial\omega$, determines the group velocity for the soliton, while the quadratic term, containing $\partial^2\epsilon_L/\partial\omega^2$, describes the dispersion of this group velocity (GVD) which causes the pulse to spread in the propagation direction. This term will counteract the tendency of the light bullet to pulse compress due to the Kerr nonlinearity and acts as the temporal analog of the transverse spatial diffraction operator (∇^2_{xy}), which counters the tendency of the light bullet to self-focus, leading to a solution that balances these forces.

For a bandlimited field of center frequency ω_0 and propagating along a direction close to the z axis, the electric field can be expanded into a plane-wave carrier and a four-dimensional envelope:

$$E=\mathscr{E}(x,y,z,t)e^{j(\omega_0 t-k_0 z)}, \tag{4}$$

where $k_0=n_0\omega_0/c$. To write the wave equation fully in the time domain, the Fourier identity $j(\omega-\omega_0)\Rightarrow \partial/\partial t$ can be applied to the dispersion terms of ϵ to yield the following expression for the scalar wave equation:

$$\begin{aligned}&\left(\frac{\partial^2\mathscr{E}}{\partial z^2}-2jk_0\frac{\partial\mathscr{E}}{\partial z}-k_0^2\mathscr{E}+\nabla^2_{xy}\mathscr{E}\right)e^{j(\omega_0 t-k_0 z)}\\&\quad-\frac{1}{c^2}\frac{\partial^2}{\partial t^2}\left[\left(\epsilon_L-j\frac{\partial\epsilon_L}{\partial\omega}\frac{\partial}{\partial t}-\frac{1}{2}\frac{\partial^2\epsilon_L}{\partial\omega^2}\frac{\partial^2}{\partial t^2}+\chi^{(3)}|\mathscr{E}|^2\right)\right.\\&\quad\left.\times\mathscr{E}e^{j(\omega_0 t-k_0 z)}\right]=0,\end{aligned} \tag{5}$$

where $\nabla^2_{xy}=\partial^2/\partial x^2+\partial^2/\partial y^2$ is the transverse part of the Laplacian. To proceed to the (3+1)D nonlinear Schrödinger equation, it is usual to assume that three groups of terms in this equation are small and can be ignored. These are (1) the slowly varying envelope approximation (SVEA) in which the second spatial derivative of the field ($\partial^2\mathscr{E}/\partial z^2$) is assumed to be small in comparison to the first derivative term ($2jk_0\partial\mathscr{E}/\partial z$); (2) the cross-term approximation in which high-order terms in the $\partial/\partial t$ polynomial resulting from the ϵE product are assumed to be dominated by the lower-order terms; the terms discarded are all time derivatives of ϵ_L greater than second degree and all time derivatives of ϵ_{NL}; and (3) the slowly varying nonlinearity approximation, in which $\partial^2(\epsilon_{NL}E)/\partial t^2$ is assumed to be equal to $-\omega_0^2\epsilon_{NL}E$. We shall also make these assumptions, but in order to establish the range of validity of the results, at the end of the next section these terms will be calculated for a set of reasonable physical parameters and the magnitude of the discarded terms will be compared to those retained.

The final NLSE can be written by defining the following normalized variables:

$$\begin{aligned}1/V_g&\equiv\frac{\partial k}{\partial\omega}\bigg|_{\omega_0}=\left(\frac{n_0}{c}+\frac{\omega_0}{c}\frac{\partial n_0}{\partial\omega}\right)=\frac{1}{n_0 c}\left(\epsilon_L+\frac{\omega_0}{2}\frac{\partial\epsilon_L}{\partial\omega}\right),\\D&\equiv-\frac{\partial^2 k}{\partial\omega^2}\bigg|_{\omega_0}=\frac{1}{\omega_0 n_0 c}\left(\epsilon_L+2\omega_0\frac{\partial\epsilon_L}{\partial\omega}+\frac{\omega_0^2}{2}\frac{\partial^2\epsilon_L}{\partial\omega^2}\right),\\\tau&=(t-z/V_g)(k_0/D)^{1/2},\\u&=(n_2/n_0)^{1/2}\mathscr{E},\\(\xi,\eta,\zeta)&=(k_0x,k_0y,k_0z).\end{aligned} \tag{6}$$

These scaled variables define a unitless position vector (ξ,η,ζ) which has been scaled by the mean wave number k_0. The definition of τ is a transformation into a group-velocity (V_g) coordinate frame which is then normalized by the group-velocity dispersion D and the wave number k_0. Positive D corresponds to AGVD and the larger the magnitude of D, the larger the resulting light bullet is in physical units, although in the normalized units it is spherical. These normalizations cause the transverse diffraction term (∇^2_{xy}) and group-velocity dispersion term ($k_0\,\partial^2k_0/\partial\omega^2\;\partial^2\mathscr{E}/\partial t^2$) to have the same form, demonstrating that diffraction and

AGVD operate in the same way to spread the soliton in the transverse and propagation directions.

The resulting normalized three-dimensional, nonlinear Schrödinger equation is

$$-j\frac{\partial u}{\partial \zeta}+\tfrac{1}{2}\nabla^2_{\xi\eta\tau}u+|u|^2u=0, \tag{7}$$

where $\nabla^2_{\xi\eta\tau}=\partial^2/\partial\xi^2+\partial^2/\partial\eta^2+\partial^2/\partial\tau^2$. In the remainder of this paper, we will write this three-dimensional, spatiotemporal Laplacian as ∇^2 for simplicity.

The three-dimensional, nonlinear Schrödinger equation has several remarkable features. The isomorphism of spatial diffraction and temporal group-velocity dispersion is complete — the temporal coordinate τ in this expression behaves the same as the transverse spatial coordinates ξ and η. We observe from the scaled variables that $|u|^2$ is equal to $n_2|E|^2/n_0$, which is the nonlinearly induced index change relative to the linear index. Thus solutions to Eq. (7) are independent of the strength of n_2; the only effect of n_2 is to scale the intensity of the electric field and thus the energy contained in the light bullets. The spatial and temporal extent of the particular solutions of the equation are also determined by Eq. (6): $\Delta x=(\lambda/2\pi)\Delta\xi$, $\Delta t=(D/k_0)^{1/2}\Delta\tau$, and $\Delta z=V_g\Delta t$, where $\Delta\xi$ and $\Delta\tau$ are normalized sizes of the soliton solutions of Eq. (7) and Δx and Δt are their mks equivalents.

We now proceed to solve for these normalized soliton solutions. If one assumes a radially symmetric (in the scaled ξ,η,τ coordinate system of the equation) propagating solution of the form $u=U(\rho)\exp(j\beta\zeta)$, Eq. (7) is simplified to an ordinary differential equation in $\rho=\sqrt{\xi^2+\eta^2+\tau^2}$.

$$\frac{1}{2}\left[\frac{\partial^2}{\partial\rho^2}+\frac{d-1}{\rho}\frac{\partial}{\partial\rho}\right]U-\beta U+U^3=0, \tag{8}$$

where d is the number of dimensions (1, 2, or 3) and β is the wave number relative to the linear wave number k_0 and is nonzero because the solitons are (nonlinearly) guided waves. This equation may be integrated (in closed form for 1D but only numerically for 2D and 3D) to determine the radial shape of the soliton. As is well known for nonlinear as well as linear guided pulses [42], the envelope will only decay to zero at infinite ρ for a discrete set of β, each of which corresponds to a mode of the system and has a number of zero crossings equal to its order, as shown in Fig. 4. The lowest-order light bullet is by far the most compact and, as shown in the figure, can be launched with orders of magnitude less energy than the higher-order modes. Also, it has been shown that the higher-order modes in a two-dimensional spatial filament stabilized with a saturating nonlinearity are unstable to angular perturbations [18]; this will probably be true of light bullets as well. For these reasons, in the remainder of this paper we will exclusively be considering the lowest-order light bullet.

The scaling relationship for these solitons is worth noting here [10]. A d-dimensional, radially symmetric soliton with radial field profile $U(\rho)$ and integrated intensity P can be scaled by a factor a via the relation

$$\tilde{U}(\rho)=aU(a\rho),\quad \tilde{P}=a^{2-d}P,\quad \tilde{\beta}=a^2\beta. \tag{9}$$

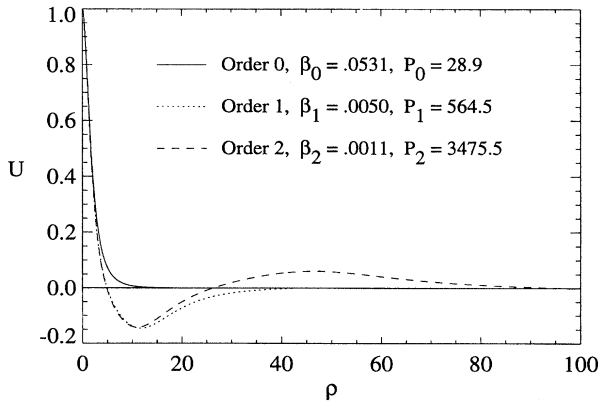

FIG. 4. Normalized light-bullet radial shapes for several orders. The decrease in β (which is the wave number *relative* to the linear wave number k_0) with increasing order indicates the higher-order solitons are less tightly guided. The legend also gives the numerically integrated intensity (which is proportional to energy) for each soliton order.

Thus to decrease the size of a one-dimensional temporal or spatial soliton by a factor of a requires a total energy or intensity which is greater by a factor of a. In two dimensions, there is no dependence of the total intensity on the size of the soliton. Finally, in three dimensions, as a soliton is decreased in radius by increasing a, the peak intensity increases by a^2, but the total energy in the light bullet *decreases* by a factor of a. These remarkable scaling relationships are ideal for creating small, intense, but low-energy pulses. As the size of the bullet approaches the wavelength in the material, the paraxial and other approximations discussed above will become increasingly invalid so the scaling to even smaller sizes would require a more complete analysis.

Unfortunately, these scaling relationships also show the light bullets to be unstable. This can be proven by examining the function $dP/d\beta$; when this quantity is positive, the zero-order soliton is stable, when it is negative or zero small perturbations from the soliton profile will grow exponentially with propagation [12]. From Eq. (9),

$$\frac{dP}{d\beta}=\left(1-\frac{d}{2}\right)\left(\frac{\beta}{\beta_{d0}}\right)^{-d/2}\frac{P_{d0}}{\beta_{d0}}\begin{cases}>0 & \text{if } d=1\\ =0 & \text{if } d=2\\ <0 & \text{if } d=3,\end{cases} \tag{10}$$

where $(P_{d0},\ \beta_{d0})$ is a particular solution of Eq. (8). Thus only one-dimensional solitons are stable. In particular, light bullets in a Kerr medium, although consistent solutions of Eq. (8), are intrinsically not robust to propagation.

Note that this instability is *not* the well-known critical collapse of the wave to an intense point focus [9]. Critical collapse events require an incident energy many times larger than that required for a fundamental soliton, while in this work the energy of the light bullets will exceed the fundamental energy by at most a factor equal to the gain, typically about 4. In contrast to the dynamics of collapse, the propagation instability is simply the evolution of the wave shape away from the eigenfunction, usually to a broader, less-

intense pulse. This evolution can be examined with numerical wave-propagation techniques, developed next.

Numerical simulations of single light bullets in Kerr media

To verify the prediction of Kerr light-bullet instability, as well as the predictions of stability for non-Kerr media later, a method is needed which will calculate the evolution of arbitrary field envelopes according to Eq. (7). Two obvious choices for this method are the finite-difference time-domain (FDTD) technique [43] and the beam-propagation method (BPM) [8]. We will choose the latter, even though it involves more assumptions about the nature of the solution, because the BPM method requires field samples spaced at three to ten times the wavelength (or at worst $\lambda/2$) , while FDTD requires many more field samples at 1/3 to 1/10 or even 1/100 wavelength spacing [44]. These different sampling densities imply a savings of three to six orders of magnitude less computer memory and time for BPM in (3+1)D simulations. The accuracy of the assumptions made in the BPM development will be addressed in the last section.

To begin, note that Eq. (7) has a formal solution

$$u(\vec{\rho},\zeta)=e^{j\int_0^{\zeta}\left[\frac{1}{2}\nabla^2+|u|^2\right]d\zeta}u(\vec{\rho},0), \quad \vec{\rho}=\xi\hat{\xi}+\eta\hat{\eta}+\tau\hat{\tau}. \tag{11}$$

To apply this exponential operator, which will advance a known field at $\zeta=0$ forward in ζ, note that the Laplacian diffraction operator ∇^2 is independent of ζ and define the average intensity for a small step in ζ of length $\Delta\zeta$ as $\bar{I}$,

$$\bar{I}\equiv\frac{1}{\Delta\zeta}\int_{\zeta}^{\zeta+\Delta\zeta}|u|^2d\zeta, \tag{12}$$

which allows us to remove the integral from Eq. (11) and write it in the form

$$u(\vec{\rho},\zeta+\Delta\zeta)=e^{\left[\frac{j}{2}\Delta\zeta\nabla^2+j\Delta\zeta\bar{I}\right]}u(\vec{\rho},\zeta). \tag{13}$$

The standard technique to solve this kind of equation [8,45] is to split the diffraction operator into a symmetric form to yield the "split-step" method:

$$u(\vec{\rho},\zeta+\Delta\zeta)\approx e^{\frac{j}{4}\Delta\zeta\nabla^2}e^{j\Delta\zeta\bar{I}}e^{\frac{j}{4}\Delta\zeta\nabla^2}u(\vec{\rho},\zeta). \tag{14}$$

The nonlinear refraction operator $e^{j\Delta\zeta\bar{I}}$ is a function of the coordinates and is easily computed and applied to the field u. The diffraction operator $e^{\frac{j}{4}\Delta\zeta\nabla^2}$ can be applied by writing the field $u(\vec{\rho},\zeta)$ as a linear combination of its linear propagation modes, Γ, which are defined to be the eigenfunctions of the diffraction operator ∇^2 with eigenvalues $-k^2$. Thus if

$$\nabla^2\Gamma(\vec{\rho},\vec{\kappa})=-k^2\Gamma(\vec{\rho},\vec{\kappa}) \tag{15}$$

then

$$u(\vec{\rho})=\int\int\int U(\vec{\kappa})\Gamma(\vec{\rho},\vec{\kappa})d^3\kappa,$$

$$U(\vec{\kappa})=\int\int\int u(\vec{\rho})\Gamma^*(\vec{\rho},\vec{\kappa})d^3\rho. \tag{16}$$

The eigenfunctions $\Gamma(\vec{\rho},\vec{\kappa})$ and eigenvalues of the Laplacian in different coordinate systems are as follows:

Rectangular:

$$\Gamma(\vec{\rho},\vec{\kappa})=\begin{cases}e^{+j(\kappa_x x+\kappa_y y+\kappa_z z)}\\ e^{-j(\kappa_x x+\kappa_y y+\kappa_z z)}\end{cases}$$
$$(k^2=\kappa_x^2+\kappa_y^2+\kappa_z^2); \tag{17a}$$

cylindrical:

$$\Gamma(\vec{\rho},\vec{\kappa})=\begin{cases}J_m(\kappa_\rho\rho)e^{-j(m\phi+\kappa_z z)}\\ Y_m(\kappa_\rho\rho)e^{-j(m\phi+\kappa_z z)}\end{cases}$$
$$(k^2=\kappa_p^2+\kappa_z^2;m=\cdots-1,0,1\ldots); \tag{17b}$$

spherical:

$$\Gamma(\vec{\rho},\vec{\kappa})=\begin{cases}j_l(\kappa_\rho\rho)Y_l^m(\theta,\phi)\\ y_l(\kappa_\rho\rho)Y_l^m(\theta,\phi)\end{cases}$$
$$(k^2=\kappa_p^2;l=0,1,2\ldots;m=-l,\ldots,l); \tag{17c}$$

where J_m and Y_m are Bessel functions, j_l and y_l are the spherical Bessel functions, and Y_l^m is the spherical harmonic [46,47]. Since these eigenfunctions of the Laplacian are guaranteed to be an orthogonal, complete set over all space, the field u can be expressed as a weighted sum of these functions of the form of Eq. (16). This transformation to the wave-vector ($\vec{\kappa}$) domain, which is commonly referred to as a Fourier transform in the rectangular coordinate system, allows us to replace the diffraction operator ∇^2 by $-k^2$. Thus the diffraction operation in the wave-vector space becomes

$$\mathscr{F}[e^{\frac{j}{4}\Delta\zeta\nabla^2}u(\vec{\rho})]=e^{-\frac{j}{4}\Delta\zeta|\vec{\kappa}|^2}U(\vec{\kappa}), \tag{18}$$

where $\mathscr{F}$ represents the transform. This transform reduces the application of the diffraction operator to a multiplication by a quadratic phase factor when the field is described in the wave-vector space. Thus alternating steps of refraction (in the "real" $\vec{\rho}$ space) and diffraction (in the "Fourier" $\vec{\kappa}$ space) will advance the field in the propagation direction. This is usually referred to as the Fourier-transform beam-propagation method.

It is straighforward to apply this method in the Cartesian space (ξ,η,τ) where the Γ functions are sinusoids and the linear expansion can be efficiently accomplished via a fast Fourier transform (FFT). This method will be applied later to investigate the interaction of multiple light bullets, but is not the most computationally efficient approach in the case of single solitons due to their spherical symmetry in the (ξ,η,τ) coordinate system. In the single-soliton case, the diffraction operator ∇^2 can be expressed in spherical coordinates and, from Eq. (17c) above, has eigenfunctions $j_0(\kappa_\rho\rho)=e^{\pm j\kappa_\rho\rho}/\rho$ for the spherically symmetric case $(m=l=0)$.

The field envelope in this case is a function of a single radial coordinate [$u=u(\rho)$] which can be transformed with the kernel $\Gamma=e^{\pm j\kappa_\rho\rho}/\rho$ into a radial spectrum of a single coordinate $U=U(\kappa_\rho)$. In comparison, the same problem expressed in Cartesian coordinates requires a field envelope which is a function of three space coordinates which is transformed via a triple integral to a Fourier-domain representation with three angular coordinates. Thus the amount of memory and computation time required to propagate a spherically symmetric field expressed in spherical coordinates are roughly the cube root of the same quantities when the problem is expressed in the Cartesian coordinate system.

The speed of the spherical-transform beam-propagation method can be further increased by noting that the transformation into and out of the spherical-harmonic space can be accomplished with FFTs:

$$\begin{aligned} U(\kappa_\rho)&=\int\int\int u(\rho)\frac{e^{-j\kappa_\rho\rho}}{\rho}\,d^3\rho \\ &=4\pi\int u(\rho)\rho e^{-j\kappa_\rho\rho}d\rho \\ &=4\pi\mathcal{F}[u(\rho)\rho], \end{aligned}$$

$$\begin{aligned} u(\rho)&=\int\int\int U(\kappa_\rho)\frac{e^{j\kappa_\rho\rho}}{\rho}\,d^3\kappa \\ &=\int\sum_l\sum_m U(\kappa_\rho)\frac{e^{j\kappa_\rho\rho}}{\rho}\,d\kappa_\rho \\ &=\frac{1}{\rho}\int U(\kappa_\rho)e^{j\kappa_\rho\rho}d\kappa_\rho \\ &=\frac{1}{\rho}\mathcal{F}^{-1}[U(\kappa_\rho)], \end{aligned} \tag{19}$$

where $\mathcal{F}$ and $\mathcal{F}^{-1}$ represent the forward and reverse FFT, respectively.

Thus, with the addition of the weighting terms defined in Eq. (19), the spherical-transform beam-propagation method looks identical to a one-dimensional Fourier-transform beam-propagation algorithm. This allows us to propagate three-dimensional, spherically symmetric field envelopes but use only the computer time and memory required for a one-dimensional simulation, reducing computation time to test the stability and robustness of a single light bullet from many hours to tens of seconds on high-performance work stations.

As predicted, such simulations show that the solitons shown in Fig. 4 are not stable when allowed to propagate. When the simulation is started with a soliton profile (as shown in Fig. 4) as an initial condition, the field does not maintain its shape with distance. Also, arbitrary pulses with energies higher than the soliton threshold do not self-stabilize into a stable soliton and a radiating continuum as is the well-known result for one-dimensional solitons. Thus additional physical terms are necessary to produce stable and robust light bullets. We now turn to the physical origin of these terms and will show that, when they are included, stable solitons can be formed.

V. ROBUST LIGHT BULLETS IN NON-KERR MEDIA

By employing the Liapunov method, several researchers have predicted the stability of three-dimensional solitons in non-Kerr media [12,48] and the bistability of light bullets in a medium with an instantaneous nonlinearity that displays two saturation plateaus has been shown numerically [21]. We have investigated two physically realizable stabilization techniques for the light bullets: a simple saturation of the nonlinear index and the inclusion of the next ($\chi^{(5)}$) term in the Taylor series expansion of the dielectric constant with intensity. Each of these methods stabilizes the solitons by limiting the peak index change. The next sections will discuss each method in turn.

A. Stabilization of solitons through saturating nonlinearity

Consider adding an instantaneous saturation term to the NLSE so that the nonlinear dielectric is of the form

$$\epsilon=\epsilon_L+\chi^{(3)}\frac{|E|^2}{1+|E|^2/|E_{sat}|^2}\,. \tag{20}$$

This form is familiar from basic laser physics as the saturation response of a two-level system [49]. For small fields, $|E|\ll|E_{sat}|$, this behaves as a conventional Kerr nonlinearity. For large fields, however, the change of index saturates at a maximum value of $\Delta\epsilon=\chi^{(3)}|E_{sat}|^2$. This will tend to flatten the index perturbation at the intense center of the light bullet.

This dielectric variation can be inserted into Eq. (8) by replacing the factor $|U|^2$ with $|U|^2/(1+|U|^2/u_{sat}^2)$. As before, this equation can be integrated to produce the fundamental soliton profiles. Figure 5 compares the fundamental soliton shape with a peak of $U(0)=1$ and no saturation ($u_{sat}=\infty$) to the eigenfunctions for materials with $u_{sat}=$ 2, 1, and 1/2. The peak field has been normalized to unity in each case so that the shapes of the solitons can be easily compared. [Note that u_{sat} scales as the field U: $\tilde{u}_{sat}=au_{sat}$, see Eq. (9)]. As expected, stronger saturation (lower u_{sat}) broadens the solitons by limiting the self-focusing effect near the center. (Reference [50] shows similar results for 2D transverse solitons.)

We can once again apply the $dP/d\beta>0$ stability test by calculating this quantity from the eigenfunction solutions of the NLSE. In agreement with the theoretical prediction of Kolokolov, and unlike light bullets in a pure Kerr material, it is now found that $dP/d\beta$ is positive (the light bullets are stable) for a sufficiently intense soliton, in particular for $U(\rho=0)\geq u_{sat}$. This is a strong modification of the Kerr-law nonlinearity since, according to this expression, the nonlinear index at $\rho=0$ must be not more than 1/2 of the Kerr value.

This stability prediction can be verified by using the spherically symmetric split-step propagation algorithm. In Fig. 6, we use this algorithm to find the propagation distance

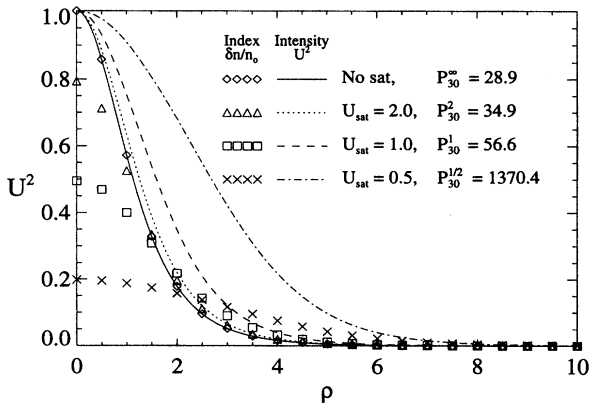

FIG. 5. Normalized light-bullet radial intensities versus the saturation level with the peak field fixed at $U(0)=1$. In contrast with the preceding figure, this plot shows intensity U^2, not field U. This allows a direct comparison with the nonlinear index, shown with symbols. Note in particular that when the peak field is equal to the saturation level [$U(0)=U_{sat}=1$], the nonlinear index at the peak is reduced to 1/2 its unsaturated level and the energy in the light bullet is nearly doubled. Finally, note that the peak field of $U(0)=1$ implies a peak nonlinear index change equal to the linear index (in the unsaturated case), which is not physically realizable. However, the scaling relations given in the last section describe how these profiles can be transformed to any peak intensity and, thus, any maximum index change.

in which the fundamental light bullet doubles its full width at half maximum size, plotted as a function of the saturation field. By fitting the resultant curve to an inverse fourth-order polynomial, we find that when the peak field [fixed at $U(0)=1$ in the plot] is greater than $0.99u_{sat}$, the distance of stable propagation asymptotically approaches infinity, which agrees well with the theoretical prediction.

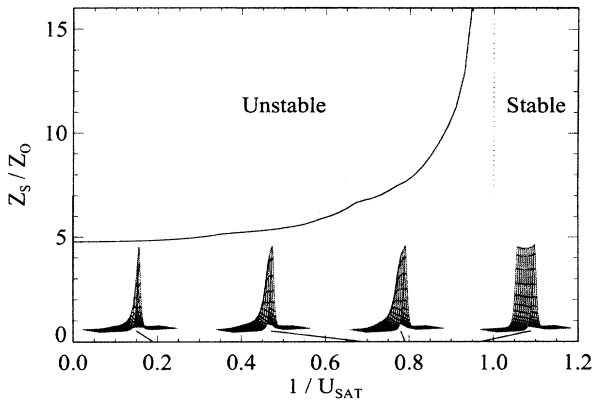

FIG. 6. Distance of stable propagation — defined as the distance in which the width of the fundamental soliton doubles — versus the saturation field for a fixed soliton peak of $U(0)=1$. The insets show the spherically symmetric envelope of the field $U(\rho)$ versus propagation distance Z at four values of u_{sat}. The distance of stable propagation approaches infinity at the predicted point of stable propagation.

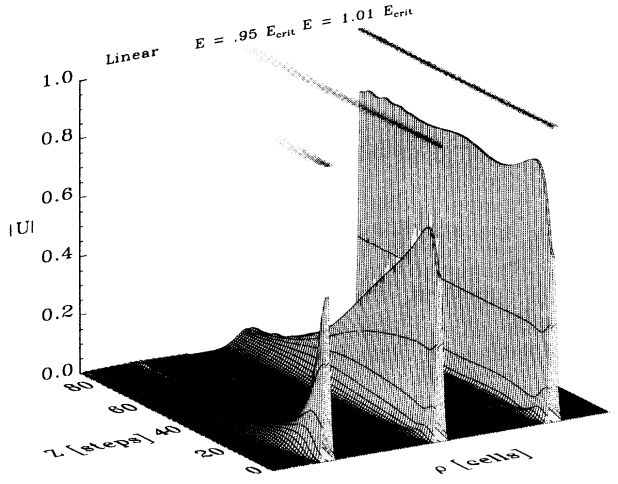

FIG. 7. Spherical BPM simulation of self-focusing 3D Gaussian pulses with two-level system saturating nonlinearity, showing a surface plot and gray-scale image of the same data. The rightmost pulse has a total energy E 1% greater than the light-bullet critical energy and thus self-focuses. The middle pulse has just less than the required energy and does not. For comparison, the leftmost pulse shows the *linear* propagation of the same pulse, demonstrating the rate of linear diffraction (ξ, η) and dispersion (τ).

These stabilized soliton profiles are attractors — initial field envelopes not too different from the fundamental shape will self-focus into the soliton and a radiation spectrum. It has even been shown that a cw beam with a temporal modulation propagating in a saturating nonlinear material with AGVD will separate into a chain of stable light bullets [23]. Figure 7 demonstrates that these stable 3D attractors in a saturating material behave just like unconditionally stable 1D solitons in a Kerr medium. In this spherical BPM simulation, a pulse with an initial 3D Gaussian profile and peak field $U(0)=1.25u_{sat}$ self-focuses into a soliton if its energy is 101% of the critical soliton energy calculated from the eigenfunction solution, but is unable to do so if its energy is just slightly below this critical value. For comparison, the propagation of the same pulse in a purely linear medium is shown on the left.

B. Stabilization of solitons through negative $\chi^{(5)}$ nonlinearity

The saturation term considered in the preceding section would occur in a two-level system, however, the nonlinear response time of typical two-level systems, involving the saturation of real particle populations, often is slower than 1 ns, which is not fast enough for this application where subpicosecond response times are required. Thus we now turn to another physical mechanism that can instantaneously limit the range of the nonlinear index — the inclusion of the third term in the power series expansion of the energy, U, of an instantaneously responding electron in a centrosymmetric potential well:

$$U=\alpha r^2+\beta r^4+\gamma r^6, \tag{21}$$

which, through the equation of motion of the electrons, leads to the power series expansion of the nonlinear index with intensity [51]:

$$\epsilon=\epsilon_L+\chi^{(3)}|E|^2+\chi^{(5)}|E|^4. \tag{22}$$

If $\chi^{(5)}$ is negative, the nonlinear dielectric can again flatten at high intensities. Applying the field scaling defined in Eq. (6), the new index expression becomes

$$n=n_0(1+|u|^2+q|u|^4), \quad q=n_0 n_4/n_2^2, \tag{23}$$

where $n_4=\chi^{(5)}/2n_0$ and q is a unitless constant expressing the strength of the fourth-order index variation which scales as $1/a^2$ [see Eq. (9)]. Dispersion terms in this equation have been left out for clarity, as they are identical to Eq. (2). Substituting this index into the normalized nonlinear Schrödinger equation gives

$$-j\frac{\partial u}{\partial \zeta}+\frac{1}{2}\nabla^2 u+|u|^2u+q|u|^4u=0. \tag{24}$$

As before, one can assume a spherically symmetric propagating solitary wave and reduce Eq. (24) to an ordinary differential equation in the radial dimension such as Eq. (8). This equation can be solved for the fundamental shapes of the solitons for various orders and values of q. This equation can be solved analytically for the one-dimensional case [52], but must again be integrated numerically for three-dimensional light bullets.

An examination of $dP/d\beta$ in this case reveals that stable propagation occurs for $q\leq -0.4$ if $U(0)=1$. Using the scaling relationships for light bullets [Eq. (9)], this can be rewritten in general as $U^2(0)\geq 0.4/(-q)$ or, in mks units, $E^2(0)\geq 0.4n_0/(-n_4)$. Numerical propagation of the spherical fundamental soliton as a function of $|q|$ produces a plot equivalent to Fig. 6 and predicts stable light-bullet propagation for $q\leq -0.41$ $[U(0)=1]$, confirming the theoretical prediction.

Figure 8 shows the spherical BPM simulation of the same initial 3D Gaussian envelope as was used in Fig. 7 in a material with $q=-0.5$ $[U(0)=1]$. The fundamental soliton profile in this case is very different from the Gaussian (unlike Fig. 7) but the same behavior occurs. As before, the critical soliton energy (E_{crit}) was found by integrating the calculated stationary eigenfunction; the simulation thus serves as a confirmation of this calculation.

It is reasonable to ask whether $q<0$ is possible in nature. Recent measurements of organic nonlinear materials such as P-toluene sulfonate (PTS) have found large positive n_2 and negative n_4 values. In PTS at 1.06 μm, $n_2=10^{-18}$ m^2/V^2 and $n_4=-2.5\times 10^{-34}$ m^4/V^4 [53], yielding $q=-425$ and stable soliton propagation for $U(0)\geq 0.03$ or $E(0)\geq 40$ MV/m. Thus the soliton formation illustrated in Fig. 8, with an initial peak field of $U(0)=0.03$, is physically correct for propagation in PTS. The light bullets used to demonstrate the dragging interactions in Sec. VII utilize a peak field of $U(0)=0.07$ and a wavelength of 1.06 μm, and are therefore well into the range of stable propagation in PTS. Thus n_4 nonlinearities of the necessary sign and magnitude exist to allow stable light-bullet propagation.

With these stabilized light-bullet profiles, we can now check the validity of the assumptions made in deriving the NLSE [Eq. (7)]. To evaluate the magnitude of the neglected terms, we require the following typical values for the physical parameters.

(1) $\lambda_0 = 1.06$ μm, due to the availability of high-power lasers at this wavelength.

(2) $n_2 = 10^{-18}$ m^2/V^2, which is the measured value for PTS at 1.06 μm [53]. This value was measured using 35 ps pulses and no discernible dispersion of the nonlinear pulse was observed. As stated in the NLSE development, we will assume an instantaneous nonlinear response.

(3) $D = 7\times 10^{-24}$ s^2/m^2, a typical value for glasses, although of the opposite sign. Thus this value would be proper for a pumped medium in which the absorption bands have been inverted to reverse the sign of the dispersion [54]. Further comments on realization of AGVD in bulk media are made in the conclusion.

(4) $n_0 = 1.5$.

We will take the soliton scaling factor a [see Eq. (9)] to be 0.07, which in Kerr media would imply a peak Kerr-induced index change of 7%. Both n_4 stabilized solitons with $q=-0.5$ and saturating-index stabilized solitons with $u_{sat}=1$ reduce this to roughly 3.5% or a peak $\Delta n\approx 0.05$ for an $n=1.5$ material. Both cases yield a fundamental soliton that is 5 μm by 5 μm by 40 fs, has a total energy of 25 pJ, and a peak intensity of 1.5 GW/cm^2.

A study of the changes in light-bullet propagation due to the various terms dropped in the 3D NLSE development is in progress. However, using the stable soliton profiles and the physical parameters given, one can evaluate these terms to estimate their importance. It is found that the terms ignored in the SVEA expansion are at most 4% of the peak field and thus are reasonable to neglect. However, dropping them does cause a subtle effect on the nature of the propagation. The linear solution of Eq. (7) implies that the propagation constant is one-half the sum of the square of the transverse spatial and temporal frequencies. This paraxial approximation is well known to be accurate only for small angles, but, as pointed out by Rothenberg [55], it also implies that the pulse propagation is separable in the transverse space and time dimensions. This separability causes the group velocity of off-axis rays to be the same as on-axis rays, which is incorrect, and can be seen in the simulation results of Sec. VII.

The expressions of the cross-term approximation are found to have peak values less than 0.6% of the field U and thus neglecting these terms should not significantly change the nature of the solutions. Note that there are third- and fourth-order time derivatives of the field in this expression which come not from higher-order dispersion terms, but from the interaction of first- and second-order dispersion terms and the second-order time derivative implicit in the

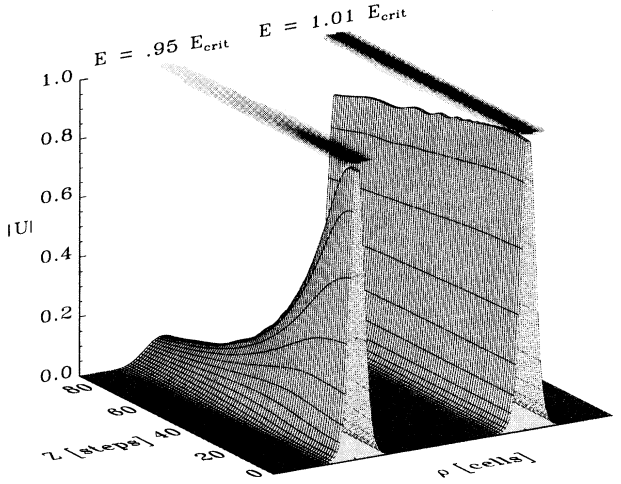

FIG. 8. Spherical BPM simulation of self-focusing 3D Gaussian pulses with $\chi^{(3)}$ and negative $\chi^{(5)}$ nonlinearities.

wave equation. Thus, when including higher-order dispersion to account for pulse asymmetry, these cross terms should also be retained [56].

The terms neglected in the slowly varying nonlinearity approximation are those that typically lead to asymmetries in the pulse envelope. The "shock" term in the slowly varying nonlinearity approximation, $\partial(|U|^2U)/\partial\tau$, has been shown to result in self-phase modulation of the wave [57], self-steepening of pulses [58], and shock-wave development [56]. It can be expanded by the product rule into two further terms, $U\partial(|U|^2)/\partial\tau$ and $|U|^2\partial U/\partial\tau$, the first of which has been shown to induce carrier downshift characteristic of the Raman effect [59]. Like the SVEA, these terms are found to be a maximum of 4% of the peak field and thus can be neglected.

We have now demonstrated that light bullets are robust under several physically reasonable situations, found their size and energy for typical experimental parameters, and checked the validity of the assumptions made in the NLSE development. In the second half of this paper, we turn to the use of these stable three-dimensional solitons as computational units through soliton interactions. First, however, we must expand the previous mathematics to include vector, rather than scalar, fields.

VI. NUMERICAL SIMULATION OF NONLINEAR VECTOR FIELDS

In order to be implemented in a complex circuit with many devices, an optical logic gate must operate independently of the relative phases of its inputs. If this were not the case, path-length changes within the machine of only fractions of a micrometer caused by heat or vibration would change the operation of the logic gate. To achieve phase insensitivity in soliton-dragging logic, we assume that the two input solitons are made up of orthogonally polarized electric fields that can only interact through nonlinearly induced index variations [2,22]. In contrast, soliton repulsion gates use copolarized beams and depend critically on the relative phase of the two signals. The difficulty with placing the solitons in orthogonal polarizations is that it complicates the nature of the interaction and it is not immediately obvious if phase-insensitive nonlinearities can be found. As will be shown in this section, with a proper choice of the orthogonal polarization states, such phase-independent interactions can indeed be achieved.

With the introduction of two distinct electric field components, the scalar wave equation [Eq. (1)] is inadequate; the complete vector nature of the problem must now be considered. For example, the simple $n=n_0+n_2I$ model of the nonlinear material is no longer valid, and the tensor nature of the nonlinear interaction must be included. Also, we must consider the tensor nature of the linear dielectric properties of the material. In order to investigate the interaction of two or more of the stabilized solitons described above, we now develop the techniques for simulating the nonlinear Schrödinger equation in both isotropic and uniaxial materials with a saturating $\chi^{(3)}$ nonlinearity or a nonsaturating nonlinear polarization expanded up through $\chi^{(5)}$. In order to maintain interactions that are only intensity (not phase) dependent, the proper optical polarizations for the solitons will have to be selected for each case.

A. Anisotropic and isotropic $\chi^{(3)}$ materials

As in the simple scalar fields case, we wish to include the effects of group velocity and group-velocity dispersion, and thus in a uniaxial material with ordinary and extraordinary indices of refraction $n_o=\sqrt{\epsilon_o}$ and $n_e=\sqrt{\epsilon_e}$

$$\epsilon_o(\omega)=\epsilon_{oL}+(\omega-\omega_0)\frac{\partial\epsilon_{oL}}{\partial\omega}\bigg|_{\omega_0}+\frac{1}{2}(\omega-\omega_0)^2\frac{\partial^2\epsilon_{oL}}{\partial\omega^2}\bigg|_{\omega_0}, \tag{25}$$

$$\epsilon_e(\omega)=\epsilon_{eL}+(\omega-\omega_0)\frac{\partial\epsilon_{eL}}{\partial\omega}\bigg|_{\omega_0}+\frac{1}{2}(\omega-\omega_0)^2\frac{\partial^2\epsilon_{eL}}{\partial\omega^2}\bigg|_{\omega_0}, \tag{26}$$

which completely specifies the *linear* dispersive response of the material. To account for the vectorial nonlinear polarization we will use the full $\chi^{(3)}$ formalism:

$$\vec{P}_{NL}=\epsilon_0\overleftrightarrow{\chi}^{(3)}\vec{E}\vec{E}\vec{E}, \tag{27}$$

where $\overleftrightarrow{\chi}^{(3)}$ is the fourth-rank nonlinear susceptibility tensor which is assumed to be instantaneous and thus nondispersive.

Together, these definitions transform the wave equation (1), in the crystallographic principal axis coordinate system, into

$$\nabla^2_{xyz}\vec{E}-\boldsymbol{\nabla}_{xyz}(\boldsymbol{\nabla}_{xyz}\cdot\vec{E})-\frac{1}{c^2}\left\{\begin{bmatrix}\epsilon_{oL}&0&0\\0&\epsilon_{oL}&0\\0&0&\epsilon_{eL}\end{bmatrix}+(\omega-\omega_0)\begin{bmatrix}\frac{\partial\epsilon_{oL}}{\partial\omega}&0&0\\0&\frac{\partial\epsilon_{oL}}{\partial\omega}&0\\0&0&\frac{\partial\epsilon_{eL}}{\partial\omega}\end{bmatrix}\right.$$
$$\left.+\frac{1}{2}(\omega-\omega_0)^2\begin{bmatrix}\frac{\partial^2\epsilon_{oL}}{\partial\omega^2}&0&0\\0&\frac{\partial^2\epsilon_{oL}}{\partial\omega^2}&0\\0&0&\frac{\partial^2\epsilon_{eL}}{\partial\omega^2}\end{bmatrix}\right\}\frac{\partial^2\vec{E}}{\partial t^2}=\frac{1}{c^2}\frac{\partial^2}{\partial t^2}(\vec{\vec{\chi}}^{(3)}\vec{E}\vec{E}\vec{E}). \tag{28}$$

Equation (28) is a fully vector partial differential equation and is rather difficult to solve analytically or numerically. It is well known, however, that the linear homogeneous version of Eq. (28) (with the right-hand side equal to zero) has two orthogonally polarized plane-wave eigenmode solutions for each direction of propagation, referred to as the ordinary and extraordinary waves. If the nonlinear polarization is assumed to be small, then these two scalar wave equations can be taken as solutions to the vector equation with the addition of a nonlinear coupling term provided by the right-hand side of Eq. (28). Under this assumption, the vector Eq. (28) can be reduced to two scalar equations for the eigenmodes of linear propagation:

$$\nabla^2_{xyz}E_{(ord)}-\frac{1}{c^2}\left[n_o^2+(\omega-\omega_0)\frac{\partial n_o^2}{\partial\omega}+\tfrac{1}{2}(\omega-\omega_0)^2\frac{\partial^2 n_o^2}{\partial\omega^2}\right]\times\frac{\partial^2E_{(ord)}}{\partial t^2}=\frac{1}{c^2}\frac{\partial^2}{\partial t^2}(\Delta\chi^{(3)}_{(ord)jkl}E_jE_kE_l),$$

$$\nabla^2_{xyz}E_{(ext)}-\frac{1}{c^2}\left[n_e(\theta)^2+(\omega-\omega_0)\frac{\partial n_e(\theta)^2}{\partial\omega}+\frac{1}{2}(\omega-\omega_0)^2\times\frac{\partial^2 n_e(\theta)^2}{\partial\omega^2}\right]\frac{\partial^2E_{(ext)}}{\partial t^2}=\frac{1}{c^2}\frac{\partial^2}{\partial t^2}(\Delta\chi^{(3)}_{(ext)jkl}E_jE_kE_l), \tag{29}$$

where $E_{(ord)}$ and $E_{(ext)}$ are the scalar electric field strengths in the ordinary and extraordinary waves and $n_e(\theta)=(\cos^2\theta/n_o^2+\sin^2\theta/n_e^2)^{-1/2}$ is the directionally dependent index of refraction of the extraordinary wave. Δ is a degeneracy factor which will depend on the physical origin of the nonlinearity. The term $\boldsymbol{\nabla}(\boldsymbol{\nabla}\cdot\vec{E})$ has been included in the homogeneous solution of Eq. (28), which is essential to capture the behavior of the fields [Eq. (29)] in anisotropic media, but the small value of this term when $\vec{E}$ is spatially varying due to the nonlinear coupling has been neglected. Also note that, in this and the following equations, the Einstein summation convention over repeated subscripts for tensor expressions is used.

In addition to the tensor nonlinearities, the propagation of the two eigenmodes described by Eq. (29) contains all of the linear physics of paraxial propagation in an anisotropic crystal, up to second order in the angle and frequency. The differences in the indices give each polarization a different phase velocity which will reveal effects such as polarization rotation and phase mismatch. The first-order expansion of this index with angle of propagation and frequency will result in different anisotropic walk off and group-velocity walk off for the two fields. Finally, the second-order expansion of the index with angle and frequency will result in differing rates of diffraction and group-velocity dispersion for the waves in each polarization. As the spatial and temporal extent of the solitons decrease, increasingly higher-order as well as mixed terms become important; in this study we have truncated the expansions at second order and limited the soliton sizes to regimes where this approximation is justified.

While the simplification of Eq. (28) to Eq. (29) has reduced us from a vector to two coupled scalar equations, we are still left with a fully vector coupling term through a fourth-order tensor. To simplify further, note that the polarization direction of the two scalar waves depends on the direction of propagation, but the two waves are always orthogonally polarized with $E_{(ord)}$ always perpendicular to both the uniaxial axis of symmetry and the direction of propagation. Thus the $\chi^{(3)}$ tensor may always be rotated to a coordinate system in which the ordinary polarization lies along the $\hat{x}$ direction and the extraordinary polarization lies along the $\hat{y}$ direction such that the electric field may be represented as

$$\vec{E}=\mathscr{E}_1\hat{x}e^{j(\omega_0t-\vec{k}_{(ord)}\cdot\vec{r})}+\mathscr{E}_2\hat{y}e^{j(\omega_0t-\vec{k}_{(ext)}\cdot\vec{r})}+\text{c.c.}, \tag{30}$$

where $\mathscr{E}_1(x,y,z,t)$ and $\mathscr{E}_2(x,y,z,t)$ are the four-dimensional envelopes and $\vec{k}_{(ord)}=n_o\omega_0/c$ and $\vec{k}_{(ext)}=n_e(\theta)\omega_0/c$ are the momentum vectors of the plane-wave carriers.

Note that this transformation is only valid for beams with small angular extents since the directions of the ordinary and extraordinary polarizations change with the direction of propagation. However, since the implementation of the beam-propagation method used in this study is also paraxial, this requirement does not further limit the applicability of the simulations.

With this definition of the electric field, the third-order nonlinear polarization terms in Eq. (29) may be written as

$$P^{(3)}_{(ord)}(\omega)=P^{(3)}_{x}(\omega)$$
$$=3\epsilon_0\chi^{(3)}_{1jkl}(\omega=\omega+\omega-\omega)E_jE_kE_l^*,$$

$$P^{(3)}_{(ext)}(\omega)=P^{(3)}_{y}(\omega)$$
$$=3\epsilon_0\chi^{(3)}_{2jkl}(\omega=\omega+\omega-\omega)E_jE_kE_l^*, \quad (31)$$

where $\{j,k,l\}$ vary over the x and y directions (indices 1 and 2). The degeneracy factor for the Kerr nonlinearity of $\Delta=3$ has been used in these expressions. A typical term of the ordinary sum will look like

$$P^{(3)}_{x}(\vec{r},t)=3\epsilon_0\chi^{(3)}_{1121}\mathscr{E}_1\mathscr{E}_2\mathscr{E}_1^* e^{-j(\vec{k}_{(ord)}+\vec{k}_{(ext)}-\vec{k}_{(ord)})\cdot\vec{r}}e^{j\omega t}$$
$$+7 \text{ other terms.} \quad (32)$$

For propagation in any direction other than the optic axis of the crystal (discussed below), the wave vectors of the ordinary and extraordinary waves are different. Since $\vec{k}_{(ext)}\neq\vec{k}_{(ord)}$, the term shown above will not be phase matched to the $\hat{x}$-polarized, propagating ordinary wave and will not contribute significantly to the macroscopic nonlinear polarization if the length of the interaction, L, is greater than $1/|(k_{(ord)}-k_{(ext)})|$. The only terms in the nonlinear polarization which will be phase matched to the propagating wave in each direction will be

$$P^{(3)}_{x}(\vec{r},t)=3\epsilon_0(\chi^{(3)}_{1111}\mathscr{E}_1\mathscr{E}_1\mathscr{E}_1^*$$
$$+2\chi^{(3)}_{1212}\mathscr{E}_2\mathscr{E}_1\mathscr{E}_2^*)e^{j(\omega t-\vec{k}_{(ord)}\cdot\vec{r})},$$

$$P^{(3)}_{y}(\vec{r},t)=3\epsilon_0(\chi^{(3)}_{2222}\mathscr{E}_2\mathscr{E}_2\mathscr{E}_2^*$$
$$+2\chi^{(3)}_{2121}\mathscr{E}_1\mathscr{E}_2\mathscr{E}_1^*)e^{j(\omega t-\vec{k}_{(ext)}\cdot\vec{r})}. \quad (33)$$

These are the familiar self-phase modulation and cross-phase modulation terms. The equation for the nonlinear index of refraction can therefore be written

$$n_{(ord)}=n_o+n^{\text{self}}_{o2}|\mathscr{E}_1|^2+n^{\text{cross}}_{o2}|\mathscr{E}_2|^2,$$
$$n_{(ext)}=n_e(\theta)+n^{\text{self}}_{e2}|\mathscr{E}_2|^2+n^{\text{cross}}_{e2}|\mathscr{E}_1|^2. \quad (34)$$

When Kleinman symmetry holds (in transparent frequency regimes far away from material resonances), these equations become nearly identical since $n^{\text{self}}_{o2}=n^{\text{self}}_{e2}$ and $n^{\text{cross}}_{o2}=n^{\text{cross}}_{e2}$.

These equations verify that the fully vector wave equation (28) including the complete tensor nature of $\chi^{(3)}$ can be described by two scalar wave equations that are coupled by simple self- and cross-phase modulation terms and are therefore completely phase independent. This simplification does require that the polarization of the two waves be selected to be the ordinary and extraordinary eigenmodes of the linear anisotropic wave equation and that the various linear and nonlinear indices be correctly calculated for the resulting polarizations.

When the direction of propagation is near the optic axis — specifically, when the angle of propagation θ is less than $\{\lambda/[2\pi L(n_o^2/n_e^2-1)]\}^{1/2}$— the ordinary and extraordinary polarizations become nearly degenerate and the phase matching of nonlinear polarization terms becomes identical to that in an isotropic material (although other optical effects such as rate of diffraction will still distinguish the two types of material). In either case, there is no difference in the ordinary and extraordinary wave vectors to enforce a phase mismatch on terms like that in Eq. (32); nonlinear polarization terms like this one make it impossible to perform phase-independent interactions for linearly polarized beams. It is possible, however, to regain a phase-independent geometry through the choice of a different basis set for the polarizations of each soliton [26,60].

First, it will be useful to derive the form of the nonlinear $\chi^{(3)}$ tensor for isotropic materials. This is tabulated in a number of sources, but in the next section we will also need the form of the $\chi^{(5)}$ tensor in isotropic materials, so we present here a simple construction method for any order. We note that in an isotropic material the tensor must be invariant to the reversal of any electric field component. This leads to the rule that a tensor component with an odd number of any particular index must be zero (e.g., $\chi_{1222}=0$), which forces all even-order (odd-rank) χ tensors to be identically zero. Secondly, the tensor must be invariant to any permutation of the indices, corresponding to a 90° rotation about some axis (e.g., $\chi_{1221}=\chi_{3113}=\chi_{2332}=\cdots$). To impose the last necessary constraint, the tensor must be invariant to rotation around an axis by an arbitrary angle, leading to the result that the complete $\chi^{(3)}$ and $\chi^{(5)}$ tensors can be written as a sum of the remaining unique terms. Thus the isotropic $\chi^{(3)}$ and $\chi^{(5)}$ tensors would be written as

$$\chi^{(3)}_{ijkl}=\chi_{1122}\delta_{ij}\delta_{kl}+\chi_{1212}\delta_{ik}\delta_{jl}+\chi_{1221}\delta_{il}\delta_{jk}, \quad (35)$$

$$\chi^{(5)}_{ijklmn}=\chi_{112233}\delta_{ij}\delta_{kl}\delta_{mn}+\chi_{112323}\delta_{ij}\delta_{km}\delta_{ln}+\chi_{112332}\delta_{ij}\delta_{kn}\delta_{lm}+\chi_{121233}\delta_{ik}\delta_{jl}\delta_{mn}+\chi_{121323}\delta_{ik}\delta_{jm}\delta_{ln}+\chi_{121332}\delta_{ik}\delta_{jn}\delta_{lm}$$
$$+\chi_{122133}\delta_{il}\delta_{jk}\delta_{mn}+\chi_{122313}\delta_{im}\delta_{jk}\delta_{ln}+\chi_{122331}\delta_{in}\delta_{jk}\delta_{lm}+\chi_{123123}\delta_{il}\delta_{jm}\delta_{kn}+\chi_{123132}\delta_{il}\delta_{jn}\delta_{km}+\chi_{123213}\delta_{im}\delta_{jl}\delta_{kn}$$
$$+\chi_{123231}\delta_{in}\delta_{jl}\delta_{km}+\chi_{123312}\delta_{im}\delta_{jn}\delta_{kl}+\chi_{123321}\delta_{in}\delta_{jm}\delta_{kl}, \quad (36)$$

where δ_{ij} is the Dirac delta function. To prove that these are the correct forms for an isotropic material, we must show that the nonlinear polarization is independent of an arbitrary rotation of the coordinate system. Writing the frequency-degenerate third-order nonlinear polarization for an arbitrary electric field,

$$\vec{E}=\mathscr{E}(e_x\hat{x}+e_y\hat{y}+e_z\hat{z})e^{j(\omega t+k_o z)}+\text{c.c.},$$

$$P_i^{(3)}=\epsilon_0\chi_{ijkl}^{(3)}E_jE_kE_l^*, \tag{37}$$

where $\mathscr{E}$ is the magnitude of the electric field and (e_x,e_y,e_z) is its unit polarization vector. The $P^{(3)}$ of Eq. (37) is written for the case of the Kerr nonlinearity, but the proof is valid for any combination of annihilation and creation operators.

Inserting the definition of $\chi^{(3)}$ above and summing over repeated indices leads to

$$\begin{aligned}P_i^{(3)}&=\epsilon_0(\chi_{1122}+\chi_{1212}+\chi_{1221})(|E_1|^2+|E_2|^2+|E_3|^2)E_i\\&=\epsilon_0(\chi_{1122}+\chi_{1212}+\chi_{1221})|\mathscr{E}|^2E_i\end{aligned}$$

or

$$\vec{P}^{(3)}=\epsilon_0(\chi_{1122}+\chi_{1212}+\chi_{1221})|\mathscr{E}|^2\vec{E}, \tag{38}$$

which shows that $\vec{P}^{(3)}$ is always parallel to $\vec{E}$ with a magnitude which is independent of direction and thus our postulation of the form of the χ tensor is verified. Precisely the same proof can be applied to $\chi^{(5)}$ to find that

$$P_i^{(5)}=\epsilon_0\left(\sum\chi\right)(|E_1|^2+|E_2|^2+|E_3|^2)^2E_i,$$

$$\vec{P}^{(5)}=\epsilon_0\left(\sum\chi\right)|\mathscr{E}|^4\vec{E}, \tag{39}$$

where, in analogy to the $\vec{P}^{(3)}$ result, $(\Sigma\chi)$ is the sum of all of the unique $\chi^{(5)}$ tensor components given in Eq. (36). Finally, note that far from material resonances, Kleinman symmetry applies and all of the χ terms in Eqs. (35) and (36) become equal, leaving only one independent constant in each tensor. In this case (which is the one used in the simulations in the next section) physically correct nonlinear materials can be modeled without a detailed knowledge of the entire tensor forms of $\chi^{(3)}$ and $\chi^{(5)}$, which are rarely adequately tabulated.

Continuing with the interaction of vector fields in an isotropic $\chi^{(3)}$ material by using the form of the tensor given in Eq. (35), the vector third-order nonlinear polarization for a Kerr nonlinearity becomes

$$\begin{aligned}\vec{P}^{(3)}&=3\epsilon_0\overleftrightarrow{\chi}^{(3)}\vec{E}\vec{E}\vec{E}^*\\&=3\epsilon_0[(\chi_{1122}+\chi_{1212})(\vec{E}\cdot\vec{E}^*)\vec{E}+\chi_{1221}(\vec{E}\cdot\vec{E})\vec{E}^*],\end{aligned} \tag{40}$$

which is not a phase-independent interaction because of the second term, which can be thought of as a traveling-wave susceptibility grating with frequency 2ω and wave vector $2k$. This can be seen by examining the coupling between an $\hat{x}$-polarized and a $\hat{y}$-polarized wave:

$$\vec{\mathscr{E}}=|\mathscr{E}_x|e^{j\phi_x}\hat{x}+|\mathscr{E}_y|e^{j\phi_y}\hat{y},$$

$$\begin{aligned}P_x^{(3)}=3\epsilon_0[&(\chi_{1122}+\chi_{1212})(|\mathscr{E}_x|^2+|\mathscr{E}_y|^2)|\mathscr{E}_x|e^{j\phi_x}\\&+\chi_{1221}(|\mathscr{E}_x|^2e^{j2\phi_x}+|\mathscr{E}_y|^2e^{j2\phi_y})|\mathscr{E}_x|e^{-j\phi_x}].\end{aligned} \tag{41}$$

The first term generates a polarization field that is in phase with the electric field and dependent only on the magnitude of the $\hat{x}$ and $\hat{y}$ fields; this term could be written as a nonlinearly induced index. In contrast, the second term is not in phase with the electric field and depends explicitly on the phases of both fields. As the phase of one electric polarization shifts, this nonlinear polarization will change in both magnitude and phase, altering the behavior of the two-field interaction by allowing a phase-dependent exchange of energy between the two polarizations.

Following the procedure of Maker and Terhune [26], we rewrite this equation in terms of circularly polarized electric fields,

$$\hat{\sigma}_\pm=\frac{\hat{x}\pm j\hat{y}}{\sqrt{2}},\quad E=E_+\hat{\sigma}_++E_-\hat{\sigma}_-, \tag{42}$$

which transforms the nonlinear polarization [Eq. (40)] into

$$\begin{aligned}\vec{P}^{(3)}=3\epsilon_0\{&[(\chi_{1122}+\chi_{1212})|E_+|^2+(2\chi_{1221}+\chi_{1122}\\&+\chi_{1212})|E_-|^2]E_+\hat{\sigma}_++[(\chi_{1122}+\chi_{1212})|E_-|^2\\&+(2\chi_{1221}+\chi_{1122}+\chi_{1212})|E_+|^2]E_-\hat{\sigma}_-\}.\end{aligned} \tag{43}$$

Thus by transforming to circular polarization states, we have reestablished a phase-independent interaction. Equation (43) serves to define self- and cross-phase modulation terms, analogous to those in Eq. (34). If the center frequency of the

light bullets is far from any material resonance, Kleinman symmetry holds and all of the independent χ terms in Eq. (35) become equal, reducing the number of unknowns in the nonlinear polarization expressions to just one. The expressions for $\vec{P}^{(3)}$ for linear and circular polarizations in isotropic media are thus as follows.

Linear polarization:

$$\vec{P}^{(3)}=9\epsilon_0\chi_{1212}\{[|E_1|^2+2/3|E_2|^2]E_1\hat{x} +[|E_2|^2+2/3|E_1|^2]E_2\hat{y}\}+\text{(phase-dependent terms)};$$

circular polarization:

$$=6\epsilon_0\chi_{1212}\{[|E_+|^2+2|E_-|^2]E_+\hat{\sigma}_+ +[|E_-|^2+2|E_+|^2]E_-\hat{\sigma}_-\}. \tag{44}$$

While the symmetries of an isotropic material allow us to deduce these forms, the values of the self- and cross-phase modulation strengths due to linearly polarized electric fields in an anisotropic material will depend on the particular crystal, its orientation, the frequency of operation, and the values of all the elements in the $\chi^{(3)}$ tensor, which are not well tabulated. However, as discussed above, Eq. (44) is the correct form for the nonlinear polarization in anisotropic crystals with sufficient birefringence and thickness since the phase-dependent terms will be phase mismatched and can be neglected. The expression for the third-order polarization due to linear fields in an isotropic medium is only included to emphasize that, even in identical isotropic materials, the choice of polarization states alters both the self- and cross-phase modulation strengths. For the case of circularly polarized fields, the single remaining independent value, $n_2^{self}=6\chi_{1212}$, can be scaled out of the propagation equations via Eq. (6) making it possible to perform a physically correct simulation of soliton interactions without using any measured $\chi^{(3)}$ values. Assuming a simple instantaneous saturation of the total nonlinearly induced index, the resulting coupled propagation equations for the case of circularly polarized electric fields in an isotropic medium are

$$-j\frac{\partial u_+}{\partial\zeta}+\frac{1}{2}\nabla^2_{\xi\eta\tau}u_+ +\frac{|u_+|^2+2|u_-|^2}{1+(|u_+|^2+2|u_-|^2)/u_{sat}^2}u_+=0,$$

$$-j\frac{\partial u_-}{\partial\zeta}+\frac{1}{2}\nabla^2_{\xi\eta\tau}u_- +\frac{|u_-|^2+2|u_+|^2}{1+(|u_-|^2+2|u_+|^2)/u_{sat}^2}u_-=0. \tag{45}$$

This form of the nonlinear index enforces a saturation of the total nonlinearly induced index seen by each polarization. This choice is somewhat arbitrary and should instead be derived from the quantum-mechanical dynamics of a particular nonlinearity. The fundamental properties of the equations, however, are independent of this choice. In particular, note that each field polarization propagates in a (3+1)-dimensional space with a three-dimensional transverse diffraction operator, $\nabla^2_{\xi\eta\tau}$, and a nonlinear index dependent only on the intensities of the two field polarizations. The particular ratio of cross- to self-phase modulation strength, 2 in this case, is determined completely by symmetry arguments for the isotropic crystal. This cross-phase modulation couples the two fields, which otherwise would support independent light-bullet solutions. Due to the choice of circular polarization states, this coupling does not depend on the relative phase of the two fields. In the next section, we expand this concept to the higher-order $\chi^{(5)}$ interaction.

B. Anisotropic and isotropic $\chi^{(5)}$ materials

In order to make use of the $\chi^{(5)}$ stabilized solitons developed in Sec. V B, we must be able to interact multiple polarizations as in the preceding section, but with the addition of the sixth-rank $\chi^{(5)}$ tensor. The preceding section has shown that in either anisotropic or isotropic materials, the interaction of two electric polarizations can be modeled as a simple self- and cross-phase modulation term which couple the two optical fields through their respective intensities alone. In this section we wish to develop the same formalism for instantaneous nonlinear polarizations expanded through the $\chi^{(5)}$ term, as required to stabilize light-bullet propagation.

First, we note that in anisotropic crystals, the arguments of the preceding section hold and terms like

$$P_x^{(5)}(\vec{r},t)=10\epsilon_0\chi^{(5)}_{112121}\mathscr{E}_1\mathscr{E}_2\mathscr{E}_1^*\mathscr{E}_2\mathscr{E}_1^* \times e^{-j(\vec{k}_{(ord)}+\vec{k}_{(ext)}-\vec{k}_{(ord)}+\vec{k}_{(ext)}-\vec{k}_{(ord)})\cdot\vec{r}+j\omega t} +31\ \text{other terms} \tag{46}$$

cannot be phase matched due to the difference in $\vec{k}_{(ord)}$ and $\vec{k}_{(ext)}$ for a sufficiently long interaction length. The degeneracy factor given by $\Delta=5!/(3!2!)=10$ is calculated for this combination of annihilation and creation operators. A study of all possible terms of the form of Eq. (46) reveals that two optical fields restricted to only the ordinary and extraordinary waves can only have intensity-dependent interactions and that these $\chi^{(5)}$ terms must be of the form

$$n_{(ord)}=n_o+n_{o4}^{\text{self}}|\mathscr{E}_1|^2+n_{o4}^{\text{cross}}|\mathscr{E}_2|^4+n_{o4}^{\text{mixed}}|\mathscr{E}_1|^2|\mathscr{E}_2|^2,$$

$$n_{(ext)}=n_e(\theta)+n_{e4}^{\text{self}}|\mathscr{E}_2|^4+n_{e4}^{\text{cross}}|\mathscr{E}_1|^4+n_{e4}^{\text{mixed}}|\mathscr{E}_1|^2|\mathscr{E}_2|^2. \tag{47}$$

Thus, when the optical polarizations are restricted to the eigenwaves of the linear crystal, vector fields can propagate and interact through intensities alone in a material displaying both $\chi^{(3)}$ and $\chi^{(5)}$ nonlinearities. The final task of this section is to show that this is also true in isotropic materials displaying a $\chi^{(5)}$ nonlinearity.

Equation (36) gives the form of the $\chi^{(5)}$ tensor in isotropic materials. The frequency-degenerate nonlinear polarization field is thus

$$\vec{P}^{(5)}=10\epsilon_0\chi^{(5)}\vec{E}\vec{E}\vec{E}\vec{E}^*\vec{E}^*=\epsilon_0\{[\chi_{112233}+\chi_{121233}+\chi_{122133}](\vec{E}\cdot\vec{E})(\vec{E}^*\cdot\vec{E}^*)\vec{E}$$
$$+[\chi_{112323}+\chi_{112332}+\chi_{121323}+\chi_{121332}+\chi_{123123}+\chi_{123132}](\vec{E}\cdot\vec{E}^*)(\vec{E}\cdot\vec{E}^*)\vec{E}$$
$$+[\chi_{122313}+\chi_{122331}+\chi_{123213}+\chi_{123231}+\chi_{123312}+\chi_{123321}](\vec{E}\cdot\vec{E})(\vec{E}\cdot\vec{E}^*)\vec{E}^*\}$$
$$=\gamma_1(\vec{E}\cdot\vec{E})(\vec{E}^*\cdot\vec{E}^*)\vec{E}+\gamma_2(\vec{E}\cdot\vec{E}^*)(\vec{E}\cdot\vec{E}^*)\vec{E}+\gamma_3(\vec{E}\cdot\vec{E})(\vec{E}\cdot\vec{E}^*)\vec{E}^*, \tag{48}$$

where γ_1, γ_2, and γ_3 are defined for convenience.

This interaction is phase dependent in the same manner as Eq. (40). To reduce it to a phase-independent geometry, we once again transform the electric field into circular polarization states via Eq. (42), which results in

$$\vec{P}^{(5)}=[\gamma_2|E_+|^2|E_+|^2+(4\gamma_1+2\gamma_2+2\gamma_3)|E_+|^2|E_-|^2$$
$$+(\gamma_2+2\gamma_3)|E_-|^2|E_-|^2]E_+\hat{\sigma}_+ +[\gamma_2|E_-|^2|E_-|^2$$
$$+(4\gamma_1+2\gamma_2+2\gamma_3)|E_+|^2|E_-|^2$$
$$+(\gamma_2+2\gamma_3)|E_+|^2|E_+|^2]E_-\hat{\sigma}_- . \tag{49}$$

This establishes that the nonlinear polarization for each electric field polarization is proportional to the electric field in the same direction and otherwise depends only on intensities. Thus these equations may be used to define fifth-order nonlinear indices of refraction that, although they are calculated differently and link circular rather than linear fields, are exactly of the form of those for the anisotropic case [Eq. (47)]. Note that for propagation along the optic axis of an anisotropic crystal, the circular basis states are only eigenpolarizations for an infinitesimal angular spectrum around the axis. Thus, in this particular case, the transverse size of the soliton will have to be sufficiently large to limit its angular spectrum to a narrow range. This restriction is similar to the requirement for small angular spectrum during off-axis propagation in an anisotropic crystal since the linear eigenpolarizations change as a function of angle. This does not mean that large angular spectrum light bullets cannot propagate and interact in these crystals, only that the techniques developed in this paper to model them are not sufficiently detailed.

With this result, we have established that, given the proper choice of the soliton polarizations and the proper calculations of the nonlinear indices of refraction from the $\chi^{(3)}$ and $\chi^{(5)}$ tensors, light-bullet interactions can always be made phase independent and can be simulated as two linearly propagating waves coupled only by intensity-dependent index functions. As in the preceding section, in isotropic materials far from any absorption resonances, Kleinman symmetry is obeyed and the constants in Eq. (47) and Eq. (49) can be calculated to within a single constant:

Linear polarization:

$$\vec{P}^{(5)}=150\epsilon_0\chi_{112233}\{[|E_1|^4+\tfrac{3}{5}|E_2|^4+\tfrac{6}{5}|E_1|^2|E_2|^2]E_1\hat{x}+[|E_2|^4+\tfrac{3}{5}|E_1|^4+\tfrac{6}{5}|E_1|^2|E_2|^2]E_2\hat{y}\}$$
$$+(\text{phase-dependent terms});$$

circular polarization:

$$=60\epsilon_0\chi_{112233}\{[|E_+|^4+3|E_-|^4+6|E_+|^2|E_-|^2]E_+\hat{\sigma}_+ +[|E_-|^4+3|E_+|^4+6|E_+|^2|E_-|^2]E_-\hat{\sigma}_-\}. \tag{50}$$

As in the preceding section, we include the expression for the fifth-order polarization induced by linearly polarized fields in an isotropic medium (even though it does not reduce to a phase-independent interaction) so that it can be compared with the phase-independent, circular basis. This equation for the fifth-order polarization induced by orthogonally circularly polarized electric fields will allow us to simulate soliton interactions mediated through sixth-order tensor nonlinearities without having to specify any of the 3^6 components of this tensor, which are (to our knowledge) not tabulated for any material. The normalized coupled propagation equations for the circularly polarized fields in this case are

$$-j\frac{\partial u_+}{\partial\zeta}+\tfrac{1}{2}\nabla^2_{\xi\eta\tau}u_+ +[|u_+|^2+2|u_-|^2$$
$$+q(|u_+|^4+3|u_-|^4+6|u_+|^2|u_-|^2)]u_+=0,$$
$$-j\frac{\partial u_-}{\partial\zeta}+\tfrac{1}{2}\nabla^2_{\xi\eta\tau}u_- +[|u_-|^2+2|u_+|^2$$
$$+q(|u_-|^4+3|u_+|^4+6|u_-|^2|u_+|^2)]u_-=0. \tag{51}$$

As in the case of a saturating nonlinearity discussed in the preceding section, the two field components propagate in a

(3+1)-dimensional space and, in the absence of the other field, each polarization will support stable light-bullet propagation, so long as $\chi^{(3)}$ is positive and $\chi^{(5)}$ is negative and assuming that sufficient power is used so that the peak nonlinear index is decreased by the negative $\chi^{(5)}$ to about half of the $\chi^{(3)}$ contribution. The two field polarizations are coupled by a nonlinear index dependent only on the intensities, not phases, of the two polarizations. The coefficients of the higher-order cross-phase and mixed-phase coupling strengths (3 and 6) are determined by the symmetry restrictions of the isotropic crystal class and allow us to perform simulations without measured values of the $\chi^{(5)}$ tensor.

The final section of this paper uses the results of the previous two sections to demonstrate light-bullet logic gates that are phase insensitive, cascadable, achieve gain, exhibit high contrast, and are logically complete.

VII. LIGHT-BULLET DRAGGING LOGIC GATES

We now have the tools to examine the feasibility of ultrafast digital optical logic based on the interaction of cross-polarized, three-dimensionally confined optical solitons. As discussed in the Introduction and shown in Fig. 3(a), the soliton-dragging logic gate described in this paper differs from other spatial soliton logic presented in the literature in that the two (or more) optical pulses are brought into coincidence in a linear material and only then are allowed to interact in the nonlinear medium. This is in contrast to the usual symmetric collision geometry, as shown in Fig. 3(c), in which the signals are allowed first to approach and then to separate entirely within the nonlinear material. The disadvantage of the collision gate is that the pump soliton is pulled first to the right and then to the left, making large displacements difficult to achieve. Numerical studies with one-dimensional spatial solitons show that collision interactions at grazing angles can achieve some gain by greatly extending the length of the interaction regime, in which the pump soliton is traveling at an angle to its initial (and final) direction. However, this is at the cost of a much larger gate length than the dragging interaction because there is an inherent tradeoff between the initial beam separation, output aperture sizes, grazing angle, and beam shift. Thus, for reasonable gate lengths, it is not possible to achieve gain (the energy of the pump exceeds the energy of the signal) with the collision interaction.

Conversely, the dragging gate presented here allows the optical pulses to approach in the linear medium where they feel no nonlinear interaction force. The pulses collide at the nonlinear material boundary and form a bound soliton pair and thus experience an immediate, strong deflection force that causes the pump to propagate at an angle which can be estimated simply by the conservation of momentum of the two solitons. As is shown in the diagram, the weaker signal soliton, after deflecting the stronger pump, usually becomes trapped and orbits around the pump. This formation of a bound soliton pair efficiently transfers the entire transverse momentum of the signal soliton to the bound pair. In contrast, the collision gate does not permanently transfer *any* transverse momentum to the pump so that after the interaction, the pump is traveling in its original direction. (In non-Kerr media or Kerr media with $d>1$ or $d=1$ and cross-polarized solitons which interact with $n^{\text{cross}}/n^{\text{self}}\neq 1$, this is not strictly true, but is nearly so.) The permanent deflection of the pump beam achieved by the dragging gate means that virtually any amount of contrast can be obtained by simply extending the distance to the pinhole aperture. Conversely, this effect can be exploited to achieve large gain; the small deflection produced by a weak signal can be amplified by a long propagation length which resolves the small angle into a large contrast. In reality, of course, this must be balanced against optical loss and latency constraints. We plan to describe the effects of optical loss, both linear and nonlinear, on the spatial soliton-dragging interaction in a future publication.

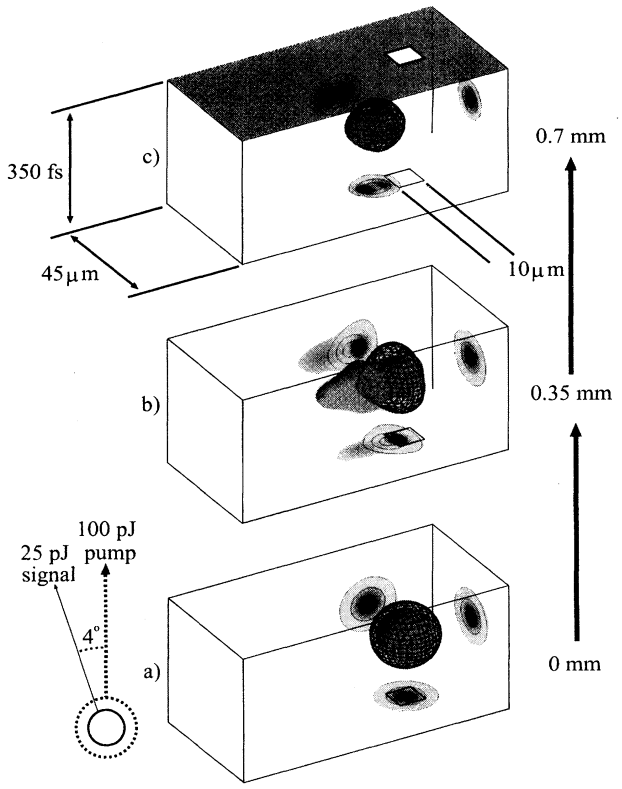

FIG. 9. Light-bullet dragging with a gain of 4 resulting in a contrast of 32 in 880 μm. The three frames shown the 100 pJ pump light bullet, rendered as a grid isosurface at 1/10 its total intensity, interacting with the 25 pJ signal light bullet, rendered as a solid isosurface at the same intensity. The energy of both the pump and the signal are projected onto the three back faces of the box and rendered as contour plots (with contours at -3, -10, and -20 dB of peak) and density maps, respectively. The position of the 10 μm square aperture is indicated and can be used (by comparison with the projected pump intensity contours) to estimate the success of the dragging operation.

A beam-propagation simulation of an asymmetric light-bullet dragging interaction is shown in Fig. 9. This shows a dragging of a circularly polarized, 5 μm$\times$5μm$\times$4μm 100 pJ pump (I_p=6 GW/cm^2) by a 25 pJ signal (I_s=1.5 GW/cm^2) in the orthogonal circular polarization in 880 μm of propagation distance using a saturating nonlinearity ($I_{sat}=I_s$) of $n_2=10^{-18}$ m^2/V^2, roughly that available from PTS [53]. The transverse size of the light bullet is easily

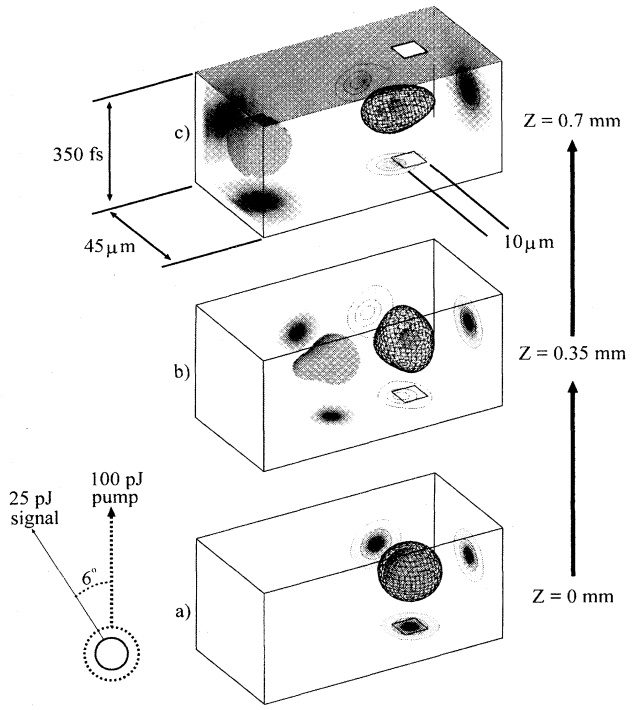

FIG. 10. Light-bullet deflection with an initial 6° intersection angle, all other parameters being the same as the preceding figure. In this case the majority of the signal energy escapes, however, it still manages to impart some transverse momentum to the pump, which propagates at an angle resulting in a contrast of 9.3 after further propagation to the the aperture located at 0.88 mm. In (c) the signal energy has collided with the reflective boundary condition of the simulation space and the reflected energy is interfering with the incident signal; this does not affect the simulation results.

achieved with high-quality optics, while the longitudinal size is several times greater than that being produced by ultrafast pulsed Ti:sapphire lasers [61,62]. The value of the AGVD is $D=7\times10^{-24}$ s^2/m^2, which could be realized from a pumped (inverted) medium [54].

Note that, at least in isotropic materials, the strength of the cross-phase modulation is proportional to this n_2 and that the proportionality constant (often labeled B in the literature) is determined only by symmetry and degeneracy factors. This proportionality constant completely determines the operation of the gate including the length and contrast — only the energy of the light bullets is scaled by the magnitude of n_2. In this case, the constant B is equal to 2, which is the value for circularly polarized fields in isotropic media with Kleinman symmetry.

The simulation space is 128 by 64 by 64 samples, is terminated by reflective boundary conditions, and is advanced a total of 100 8.8 μm propagation steps. In normalized values, the peak signal soliton field is $U(0)=0.071$, which translates to a maximum Kerr-induced index of $5\times10^{-3}n_0$. However, the saturation of this nonlinearity with u_{sat} set equal to $u(0)$ reduces this by a factor of 2 to $2.5\times10^{-3}n_0$.

In the bottom frame of the figure, the 25 pJ signal soliton, rendered as a solid isosurface at 1/10 of its peak intensity, is initially overlapping (in both space and time) the 100 pJ pump light bullet, represented by a grid isosurface at the same intensity level. As the two solitons propagate upward, with the signal tilted at an initial 4° angle, the pump is pulled out of the 10 micrometer aperture to implement the inversion or switching operation. The contrast of the gate, defined as the amount of energy in a fundamental soliton (25 pJ) over the total pump energy that escapes the aperture, exceeds 32 in a gate length of only 880 μm. Note that in the absence of the signal, the pump propagates straight up and 96% of the pump energy passes through, which can then be fanned out as a logically true signal for subsequent gates. This interaction implements a simple high-contrast inverter with gain which completely restores the logical and physical characteristics of the information carrier.

If the initial angle is increased to 6°, the pump and signal solitons do not form a bound pair, as shown in Fig. 10. In this case, a deflection, rather than dragging, interaction (see Sec. II) is implemented. Even though the two solitons separate, the signal still manages to impart a permanent transverse momentum to the pump. After a sufficient propagation distance, this causes the pump to move out of the path of the aperture, implementing the desired switching function with a contrast of 9. This contrast can be increased by simply lengthening the gate beyond the 880 μm simulated here.

Figure 11 summarizes the operation of this light-bullet logic gate by plotting the contrast of the gate versus initial interaction angle and gate length for saturation and negative $\chi^{(5)}$ stabilized light bullets in both isotropic and anisotropic media. (The details of the simulations are the same as those given above, except as noted in the figure caption.) As was developed previously, circularly polarized solitons in an isotropic material with Kleinman symmetry interact independent of their relative phase and the cross-phase modulation strengths can be determined completely by symmetry [see Eq. (44) and Eq. (50)]. In anisotropic materials, however, the magnitude of these cross-phase terms depends on the particular crystal, its orientation, and the soliton color. Since these values are not well tabulated, particularly in the case of $\chi^{(5)}$, the simulations of light-bullet interaction in anisotropic materials in Figs. 11(c) and 11(d) were performed with linear polarizations but with the cross-phase modulation strengths for an isotropic crystal. The similarity of the four plots serves to demonstrate that, though the quantitative behavior of the switch depends on these ratios, the qualitative behavior does not change.

In particular, the figure shows that there is an optimum angle for the dragging interaction. As illustrated in Fig. 9, this occurs when the signal nearly escapes from the attractive potential well formed by the pump. In this case, a saturating nonlinearity in an isotropic material, the large ratio of cross- to self-phase modulation makes possible a large contrast in less than a millimeter with an optimum angle of 4°. In contrast, all other cases have a somewhat reduced cross-phase modulation strength, and thus the optimum angle of interaction drops and a larger gate length is required to achieve the same contrast.

This figure also illustrates the robustness of the gate to minor angular misalignments — there is no critical angle for operation but rather a gradual change from one type of interaction to the next. When the interaction angle equals zero, this is the soliton breathing gate mentioned in the Introduc-

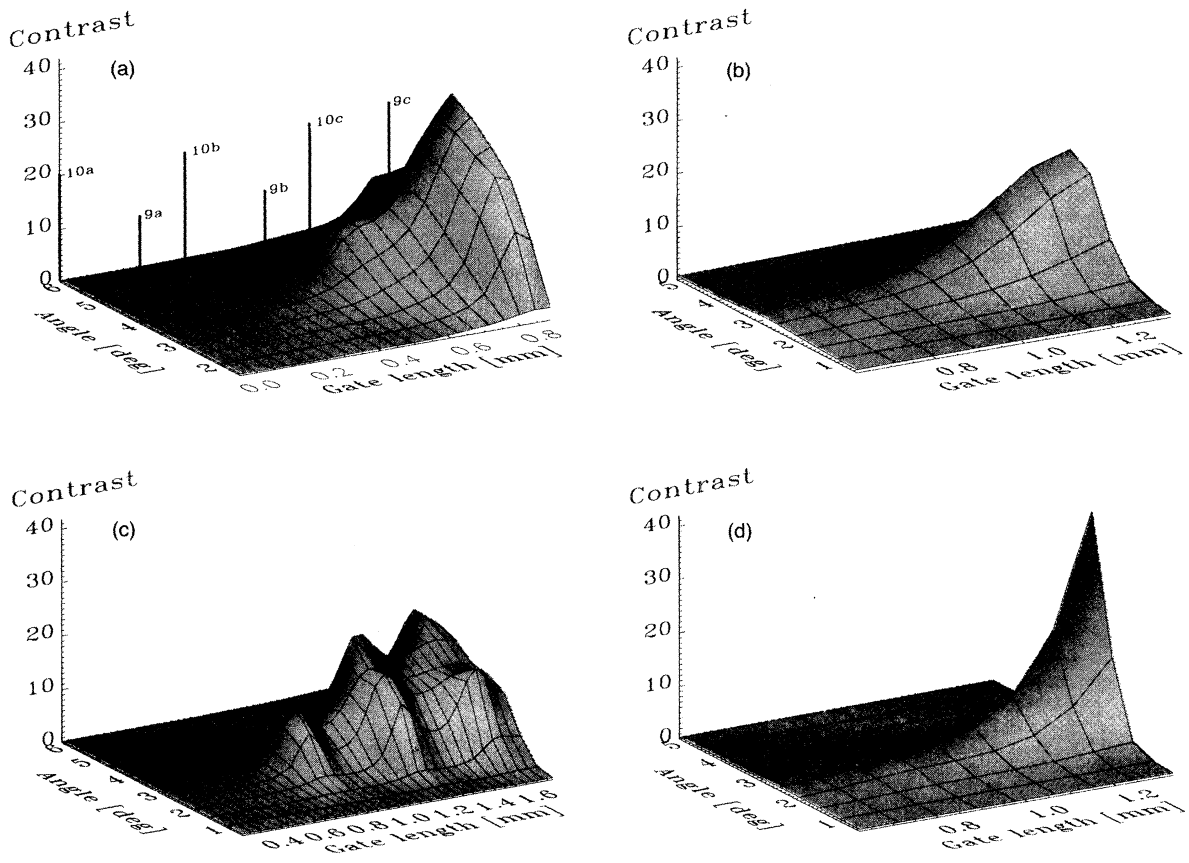

FIG. 11. Contrast equal to energy of fundamental over pump energy leaked through 10 μm square aperture versus initial interaction angle and propagation distance for two different linear isotropic nonlinear media and two different polarization basis sets (note that the angle and distance scales vary between plots). For the saturating media [(a) and (c)] $U_{sat} = 1$; for the $\chi^{(5)}$ media [(b) and (d)] $q = -0.5$. The soliton scaling relation is used to yield an actual peak field, in the normalized units, of $U(0) \approx 0.15$ in both cases, which was chosen to yield a fundamental soliton with the size described in the text. The cross- to self-phase modulation ratio for circular polarizations in an isotropic medium [(a) and (b)] was derived in the text; this choice was shown to result in phase-independent interactions. Linear polarizations in isotropic media [(c) and (d)] are phase dependent, and thus an anisotropic crystal is required. However, the cross-phase modulation strengths in this case depend on the particular anisotropic crystal, its orientation, and the frequency of the optical carrier. As an illustrative example, (c) and (d) show the contrast for a phase-independent interaction utilizing the nonlinear index ratios for an isotropic material. No linear anisotropic behaviors (such as walk off) were included. The labels on (a) indicate the frames rendered in the previous two figures.

tion, which achieves a contrast of 3 [from Fig. 11(a)]. Conversely, when the interaction angle is very large, the two solitons do not form a bound pair and quickly separate, implementing the deflection operation, as illustrated in Fig. 10. In the absence of absorptive loss (which has not been included in this study) the contrast of the gate can be increased simply by making the gate longer. In reality, this must be balanced against the loss of pump and signal energy in the length of the gate.

The interaction shown in these figures can be used as a phase-insensitive inverter with a gain of 4 and contrast greater than 32 by placing an aperture in the output plane that would pass the undeflected pump (as indicated by the 10 μm square in the figures). This implements a logical inverter, two of which can be placed in series to create a two-input NOR gate [2,39,63,22,64]. Since NOR is logically complete, any combinatorial logic function can be implemented with this gate. Note that although the latency of the 0.88 mm gate (for a linear index of 1.5) is about 4 ps, the time occupied by a single dragging operation is much shorter. If operations were pipelined within the gate spaced at ten times the temporal duration of the bullets to avoid intersymbol interference, a single computation would occur each 200 fs. These gates can be operated in parallel in a uniform block of nonlinear material (except for the apertures); distributing them transversely at ten times the soliton width and longitudinally at twice the gate length yields a density of gates of one-half million per cubic inch. Coupled with the pipelined operation, this yields an (extremely optimistic) upper bound of 2.5×10^{18} bit operations per cubic inch per second.

The multidimensional nature of the light-bullet dragging logic gate can be utilized to create a simpler, single-stage NOR with fan in by allowing three solitons to interact, as shown in Fig. 12. This simulation is identical to the previous, one-signal results, except that two signals are present, one tilted towards $\hat{x}$, and the other towards $\hat{y}$. Since there are

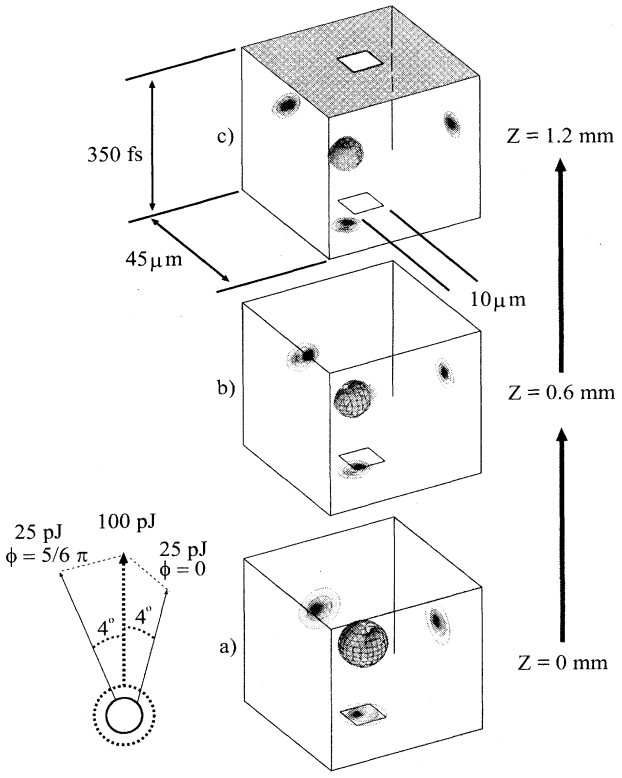

FIG. 12. Simulation of a single-stage NOR gate with a fan in of 2. The signals, in the same polarization, are 5/6 π out of phase and produce an initial interference null. Some energy is radiated, but the majority forms a complex, bound vector soliton which propagates out along the diagonal between $\hat{x}$ and $\hat{y}$.

only two available orthogonal electric field polarizations, the two signal solitons (which are chosen to be in the same polarization) must now interfere. The figure shows nearly the worst-case scenario in which the two signals are $5/6\pi$ out of phase such that there is an initial interference null on the diagonal axis. Since the linear resolvability of these two signal solitons is $\sqrt{2}$, there is only one fringe with the beam profile. As would be expected, the pump is dragged by both signals along the diagonal. Although the operation of the gate is degraded by the signals being out of phase, it operates successfully at all relative phases. This degradation can be overcome by using a slightly longer gate length, as is shown in Fig. 13. Thus this arrangement forms a phase-independent, single-stage, two-input NOR gate; if one or both titled signals are present, the pump is dragged to the side in x, in y, or diagonally in xy so that almost no power passes through the aperture at the output of the nonlinear material. If none of the signals is present, the undragged pump passes through the output aperture and is available as a signal to switch subsequent stages.

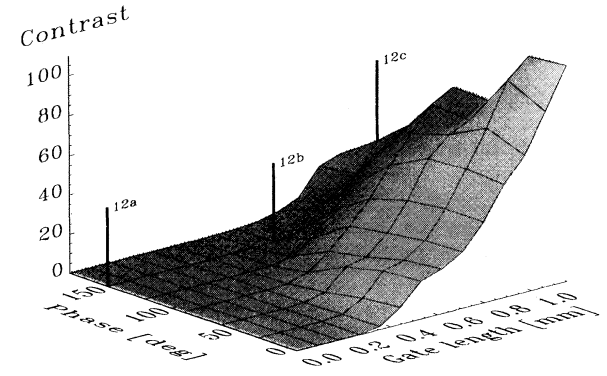

FIG. 13. Contrast of two-input single-stage NOR as a function of gate length and relative phase of the two signals. The labels show the positions of the frames rendered in the preceding figure.

A two-input, single-stage NOR implemented by soliton dragging in a one-dimensional temporal interaction has been reported [38]. However, the linear interference between the two copolarized and copropagating signals is much more serious in this case, making the operation of the gate strongly phase sensitive.

The design of the multiple-input light-bullet dragging logic gate can be extended to larger numbers of inputs by arranging a number of tilted inputs to be on a cone extending over 90° between $\hat{x}$ and $\hat{y}$ (so that no signal drags in a direction that opposes another). We have simulated a four-input NOR gate like the two-input gate above with similar results. This flexibility in the fan in strongly relaxes the constraints on a digital systems designer using these gates.

The astute reader will note that the signal energy which escapes in the simulation results (e.g., Fig. 10) does not fall behind due to what should be its decreased group velocity in the $\hat{z}$ direction. This is because the development of the NLSE assumed a single group velocity, independent of direction of propagation and thus the soliton propagating at a 6° angle does not fall behind the pump as it should [55]. This inaccuracy can be minimized if one considers the solitons to be propagating symmetrically around the $\hat{z}$ axis (i.e., at +3° and −3°), which is just as valid. However, it has been suggested that this lack of variation of the group velocity away from the propagation axis invalidates the entire NLSE approach to space-time self-focusing [65]. Note that the variation of *phase* velocity with direction is correctly handled by the NLSE.

VIII. DISCUSSION AND SUMMARY

Light bullets are an exciting physical phenomenon that offer great promise as computing and logic elements. To motivate their use in a digital optical computing system, we have reviewed the types of optical solitons including spatial, temporal, and spatiotemporal solitons confined in one, two, or three dimensions, as well as bright, dark, and combined bright-dark envelopes. Since there are a limited number of ways in which any two of these solitons can interact, a unified description of the possible two-soliton interactions in one, two, or three dimensions and the properties of each were introduced.

The types of solitons and the properties of the possible soliton interactions were then compared to the requirements for all-optical digital logic, in particular the need for a three-terminal, cascadable device with gain and phase insensitivity. On the basis of this comparison, it was shown that light bullets — three-dimensional self-contained optical solitons in homogeneous media — support highly parallel, fast, low-

energy switching. The soliton-dragging interaction, in which two solitons collide at the beginning of the nonlinear material and form a bound pair, was shown to fit the requirements for three-terminal, phase-insensitive logic with gain. Thus light-bullet dragging logic gates appear to have almost all the requisite features to implement large-scale digital optical logic.

Starting first with the scalar wave equation, we derived the field profiles of the fundamental and higher-order light bullets. From the eigenequation for these solitary waves, the amplitude scaling relation was derived and used to show that light bullets must be unstable to propagation in a purely Kerr medium. To verify this prediction, we developed a simple, efficient beam-propagation method based on the eigenfunction expansion of the nonlinear wave equation in any coordinate system. This was specialized to the case of 3D, spherically symmetric envelopes, and used to construct an efficient BPM algorithm which uses only 1D FFTs — this algorithm confirmed the radial instability of light bullets in a Kerr material.

To stabilize the propagation of light bullets, we investigated two non-Kerr media: a material with an instantaneous saturation of the nonlinear index and a medium with both positive second-order and negative fourth-order dependence of the index on electric field, both of which tend to decrease the nonlinear index for high optical intensities near the center of the light bullet. In both cases, a modified nonlinear Schrödinger equation was derived and used to find the shape of the soliton envelopes as a function of the strength of the non-Kerr perturbation. These results revealed the ranges for stable soliton propagation via Kolokolov's stability formula which was found to be in excellent agreement with our spherical BPM simulations. In both cases, it was found that the light bullets have to be sufficiently intense that the nonlinearly induced index at the center is roughly half of what it would have been in a purely Kerr material. These stable solitons were shown to be attractors in phase space by simulating soliton formation from arbitrary 3D envelopes. The existence and value of a threshold energy for soliton formation, derived directly from the modified NLSE, was also verified numerically.

In order to simulate the dragging interaction of these robust light bullets, we then developed a beam-propagation method from the fully vector wave equation for vector fields in anisotropic materials with up to sixth-order tensor-mediated nonlinearities. To use realistic nonlinear tensors, this was specialized to the case of isotropic crystals where the large number of symmetries was used to reduce the χ tensors to a single independent value. To find the form of the higher-order χ tensor, we introduced a simple formalism to find such tensors of any order in an isotropic crystal. With these tensor forms, it was shown that, with proper choice of soliton polarizations, phase-independent interactions can be arranged in both saturating and negative $\chi^{(5)}$ materials and in both isotropic and anisotropic media.

These techniques were used to simulate the operation of light-bullet dragging logic in four different materials classes. Utilizing n_2 values from currently available nonlinear materials, we demonstrated the possibility of NOT, two-input NOR, and four-input NOR logic gates in a volume of roughly 40 μm $\times$ 40 μm $\times$ 880 μm. The gates have a gain of 4, contrast of 32, switching energy of 25 pJ, and clock rate of 5 THz. These power levels must be decreased through enhanced χ^3 for practical applications [66].

A number of questions remain to be answered about this device. Additional theoretical investigation of the light-bullet phenomenon via the inclusion of higher-order dispersion, diffraction, and nonlinear terms should refine the predictions made in this work. Also not considered in this work is the vector nature of guided e.m. fields which imposes restrictions on the electric field mode shape and polarization. These effects have been examined for 2D filaments [67] and need to be extended to the case of 3D light bullets. These refinements should not change the basic asymmetry of the dragging interaction in which the weak signal bullet drags the strong pump to one side and it is reasonable to assume that the form and properties of the gates will remain essentially unchanged.

Experimental verifications of the light-bullet phenomenon need to be performed; the simulations used in this paper indicate that this should be possible if a material with a strongly negative n_4 and anomalous GVD can be fabricated. Recent measurements of PTS [53] at 1.06 μm have revealed an n_2 of 10^{-18} $(\text{m/V})^2$ with a very large, negative n_4 of 2.5×10^{-34} $(\text{m/V})^4$ [53]. This value of n_2 was the one used in the simulations, thus 25 pJ fundamental solitons should be possible. Enhanced nonlinear materials may provide an order-of-magnitude increase of n_2 with only a slight increase of absorption and nonlinear response time, allowing pJ-scale light bullets, approaching practical energies for optical switching applications.

Unfortunately, PTS, like most transparent bulk materials, exhibits normal GVD. The most promising technique to overcome this problem is to periodically layer the media with alternating linear indices in the propagation direction to create a "photonic band gap" [68]. By operating near but not in the forbidden band, AGVD can be created. Theoretical investigation of the interaction of material and grating GVD as well as the 3D, vector nature of the problem are still in progress. Other approaches to achieving AGVD include using bulk form birefringence due to transmission grating structures, pumping the medium to turn absorption bands into gain, and NGVD into AGVD [54] and parametric gain [11].

To make good use of these gates, systolic arrays or a similar three-dimensional data-flow technique need to be developed to take advantage of this highly parallel logic device. For example, a folded architecture has been designed that, rather than absorbing the solitons after they interact, allows them to propagate out of the device to be dissipated remotely. This "optical cooling" separates the logical decision from the energy dissipation required to make the decision, significantly simplifying the cooling problem. The possibility of constructing all-optical, light-bullet dragging logic circuits with millions of gates operating at THz clock speeds is strong motivation for the continued materials, theoretical, and systems research necessary to realize these devices.

ACKNOWLEDGMENTS

This work was supported by NSF Grant No. ECS 92-58088 and R. M. is supported by DOD Grant No. DAAL03-92-G-0351.

[1] L. F. Mollenauer, R. H. Stolen, and J. P. Gordon, Phys. Rev. Lett. **45**, 1095 (1980).
[2] M. Islam, Opt. Lett. **14**, 1257 (1989).
[3] R. Y. Chiao, E. Garmire, and C. H. Townes, Phys. Rev. Lett. **13**, 479 (1964).
[4] V. I. Talanov, Pis'ma Zh. Éksp. Teor. Fiz. **2**, 222 (1965) [JETP Lett. **2**, 138 (1965)].
[5] P. L. Kelley, Phys. Rev. Lett. **15**, 1005 (1965).
[6] V. E. Zakharov and A. B. Shabat, Zh. Eksp. Teor. Fiz. **61**, 118 (1971) [Sov. Phys. JETP **34**, 62 (1972)].
[7] J. S. Aitchison, A. M. Weiner, Y. Silberberg, M. K. Oliver, J. L. Jackel, D. E. Leaird, and E. M. Vogel, Opt. Lett. **15**, 471 (1990).
[8] M. D. Feit and J. A. J. Fleck, J. Opt. Soc. Am. B **5**, 633 (1988).
[9] J. Rasmussen and K. Rypdal, Phys. Scr. **33**, 481 (1986).
[10] Y. Silberberg, Opt. Lett. **15**, 1282 (1990).
[11] A. Blagoeva, S. G. Dinev, A. A. Dreischuh, and A. Naidenov, IEEE J. Quantum Electron. **27**, 2060 (1991).
[12] A. A. Kolokolov, J. Appl. Mech. Tech. Phys. **3**, 426 (1973).
[13] K. Hayata and M. Koshiba, Opt. Lett. **17**, 841 (1992).
[14] V. E. Zakharov, Zh. Eksp. Teor. Fiz. **53**, 1735 (1967) [Sov. Phys. JETP **26**, 994 (1968)].
[15] V. E. Zakharov and A. M. Rubenchik, Zh. Eksp. Teor. Fiz. **65**, 997 (1973) [Sov. Phys. JETP **38**, 494 (1973)].
[16] Y. Chen and J. Atai, Opt. Lett. **20**, 133 (1995).
[17] J. Robinson and D. Andersen, Opt. Comput. Processing **2**, 57 (1992).
[18] J. M. Soto-Crespo, D. R. Heatley, and E. M. Wright, Phys. Rev. A **44**, 636 (1991).
[19] M. Karlsson, Phys. Rev. A **46**, 2726 (1992).
[20] A. W. Snyder, D. J. Mitchell, L. Poladian, and F. Ladoucer, Opt. Lett. **16**, 21, (1991).
[21] D. Edmundson and R. Enns, Opt. Lett. **17**, 586 (1992).
[22] S. Blair, K. Wagner, and R. McLeod, Opt. Lett. **19**, 1943 (1994).
[23] N. Akhmediev and J. M. Soto-Crespo, Phys. Rev. A **47**, 1358 (1993).
[24] A. B. Aceves and C. De Angelis, Opt. Lett. **18**, 110 (1993).
[25] J. G. A. Swartzlander and C. Law, Phys. Rev. Lett. **69**, 2503 (1992).
[26] P. Maker and R. Terhune, Phys. Rev. **137**, A801 (1965).
[27] A. P. Sheppard and M. Haelterman, Opt. Lett. **19**, 859 (1994).
[28] D. Edmundson and R. Enns, Opt. Lett. **18**, 1609 (1993).
[29] J.-R. Bian and A. K. Chan, Microwave Opt. Technol. Lett. **4**, 575 (1991).
[30] J. Aitchison, A. Weiner, Y. Silberberg, D. Leaird, M. Oliver, and J. Jackel, Opt. Lett. **16**, 15 (1991).
[31] X. Cao and D. Meyerhofer, Opt. Lett. **19**, 1711 (1994).
[32] T.-T. Shi and S. Chi, Opt. Lett. **15**, 1123 (1990).
[33] S. R. Skinner, G. R. Allan, and D. R. Andersen, IEEE J. Quantum Electron. **27**, 2211 (1991).
[34] P. Mamyshev, A. Villeneuve, G. I. Stegeman, and J. Aitchison, Electron. Lett. **30**, 726 (1994).
[35] G. E. Torres-Cisneros, J. J. Sanches-Mondragon, and V. A. Vysloukh, Opt. Lett. **18**, 1299 (1993).
[36] S. R. Friberg, Appl. Phys. Lett. **63**, 429 (1993).
[37] M. Shalaby and A. Barthelmy, Opt. Lett. **16**, 1472 (1991).
[38] M. Islam, Opt. Lett. **15**, 417 (1990).
[39] K. Wagner and R. McLeod, in *OSA Annual Meeting Technical Digest, 1992* (Optical Society of America, Washington, D.C., 1992), Vol. 23, p. 129.
[40] R. W. Keyes, Opt. Acta **32**, 525 (1985).
[41] C. R. Menyuk, J. Opt. Soc. Am. B **5**, 392 (1988).
[42] H. A. Haus, Appl. Phys. Lett. **8**, 128 (1966).
[43] K. S. Yee, IEEE Trans. Antennas Propag. **AP-14**, 302 (1966).
[44] R. W. Ziolkowski and J. B. Judkins, J. Opt. Soc. Am. B **10**, 186 (1993).
[45] J. A. J. Fleck and M. D. Feit, J. Opt. Soc. Am. B **73**, 920 (1983).
[46] *Handbook of Mathematical Functions*, edited by M. Abramowitz and I. A. Stegun (Dover Publications, New York, 1984).
[47] R. Eisberg and R. Resnik, *Quantum Physics of Atoms, Molecules, Solids, Nuclei, and Particles* (Wiley, New York, 1976).
[48] N. G. Vakhitov and A. A. Kolokolov Izv. Vyssh, Uchebn. Zaved. Radiotiz. **16**, 1020 (1973) [Sov. Radiophys. **9**, 261 (1973)].
[49] L. Allen and J. Eberly, *Optical Resonance And Two-Level Atoms* (Dover, New York, 1988).
[50] Y. Chen, Opt. Lett. **16**, 4 (1991).
[51] A. H. Piekara, J. S. Moore, and M. S. Feld, Phys. Rev. A **9**, 1403 (1974).
[52] C. D. Angelis, IEEE J. Quantum Electron. **30**, 818 (1994).
[53] B. L. Lawrence, M. Cha, W. E. Toruellas, G. I. Stegeman, S. Etemad, G. Baker, and F. Kajzar, Appl. Phys. Lett. **64**, 2273 (1994).
[54] G. Khitrova, H. Gibbs, Y. Kawamura, H. Iwamura, T. Ikegami, J. E. Sipe, and L. Ming, Phys. Rev. Lett. **70**, 920 (1993).
[55] J. E. Rothenberg, Opt. Lett. **17**, 1340 (1992).
[56] E. Bourkoff, W. Zhao, R. Joseph, and D. Christodoulides, Opt. Lett. **12**, 272 (1987).
[57] N. Tzoar and M. Jain, Phys. Rev. A **23**, 1266 (1981).
[58] D. Anderson and M. Lisak, Phys. Rev. A **27**, 1393 (1983).
[59] Y. Kodama and K. Nozaki, Opt. Lett. **12**, 1038 (1987).
[60] A. L. Berkhoer and V. E. Zakharov, Zh. Eksp. Teor. Fiz. **58**, 903 (1970) [Sov. Phys. JETP **31**, 486 (1970)].
[61] A. Stingl, C. Spielmann, and F. Krausz, Opt. Lett. **19**, 204 (1994).
[62] M. T. Asaki, C.-P. Huang, and D. Garvey, Opt. Lett. **18**, 977 (1993).
[63] K. Wagner and R. McLeod, in *Optical Computing Technical Digest, 1993* (Optical Society of America, Washington, D.C., 1993), Vol. 7, p. 305.
[64] R. McLeod, S. Blair, and K. Wagner, in *Optical Computing, 1994* (Institute of Physics, Philadelphia, 1994), Vol. 139, p. 657.
[65] N. Akhmediev, A. Ankiewics, and J. M. Soto-Crespo, Opt. Lett. **18**, 411 (1993).
[66] R. DeSalvo, D. Hagan, M. Sheik-Bahae, G. Stegeman, E. Van Stryland, and H. Vanherzeele, Opt. Lett. **17**, 28 (1992).
[67] Y. Chen, IEEE J. Quantum Electron. **27**, 1236 (1991).
[68] C. M. de Sterke and J. E. Sipe, Phys. Rev. A **38**, 5149 (1988).

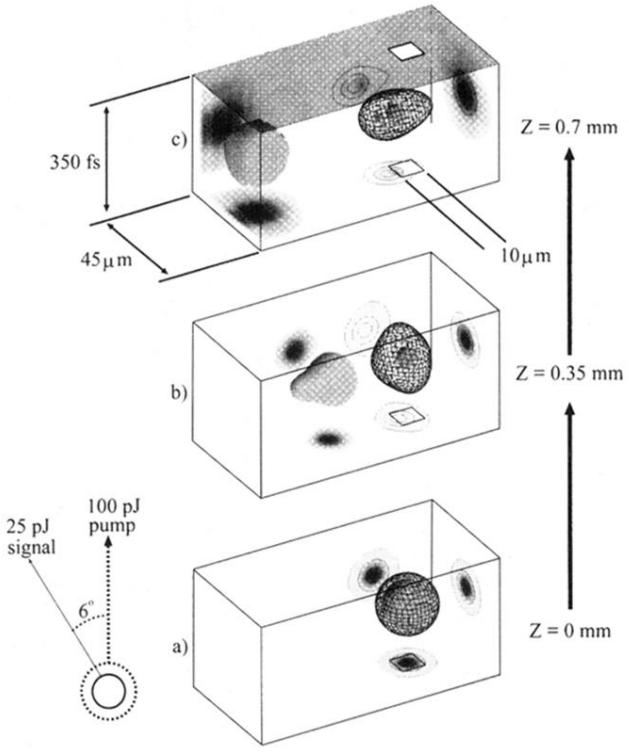

FIG. 10. Light-bullet deflection with an initial 6° intersection angle, all other parameters being the same as the preceding figure. In this case the majority of the signal energy escapes, however, it still manages to impart some transverse momentum to the pump, which propagates at an angle resulting in a contrast of 9.3 after further propagation to the the aperture located at 0.88 mm. In (c) the signal energy has collided with the reflective boundary condition of the simulation space and the reflected energy is interfering with the incident signal; this does not affect the simulation results.

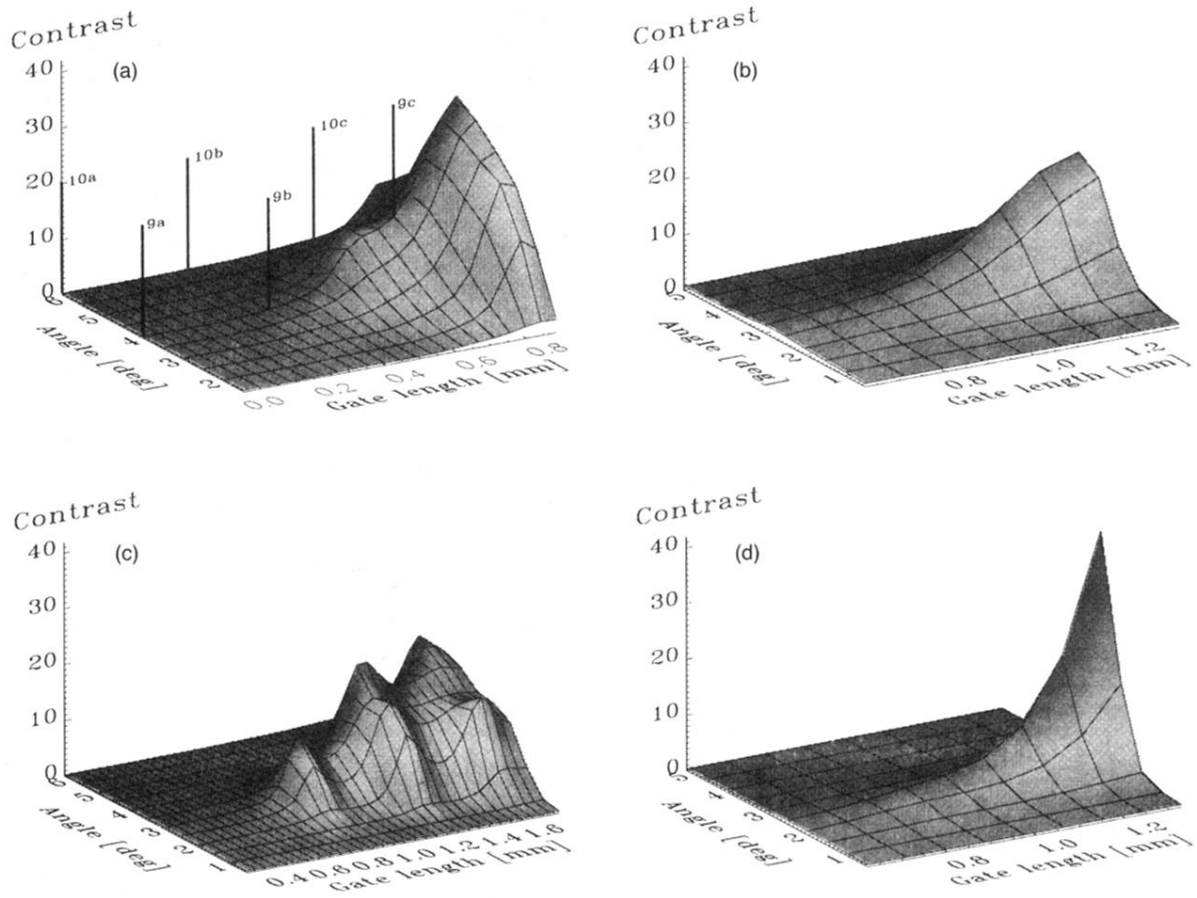

FIG. 11. Contrast equal to energy of fundamental over pump energy leaked through 10 μm square aperture versus initial interaction angle and propagation distance for two different linear isotropic nonlinear media and two different polarization basis sets (note that the angle and distance scales vary between plots). For the saturating media [(a) and (c)] $U_{sat} = 1$; for the $\chi^{(5)}$ media [(b) and (d)] $q = -0.5$. The soliton scaling relation is used to yield an actual peak field, in the normalized units, of $U(0) \approx 0.15$ in both cases, which was chosen to yield a fundamental soliton with the size described in the text. The cross- to self-phase modulation ratio for circular polarizations in an isotropic medium [(a) and (b)] was derived in the text; this choice was shown to result in phase-independent interactions. Linear polarizations in isotropic media [(c) and (d)] are phase dependent, and thus an anisotropic crystal is required. However, the cross-phase modulation strengths in this case depend on the particular anisotropic crystal, its orientation, and the frequency of the optical carrier. As an illustrative example, (c) and (d) show the contrast for a phase-independent interaction utilizing the nonlinear index ratios for an isotropic material. No linear anisotropic behaviors (such as walk off) were included. The labels on (a) indicate the frames rendered in the previous two figures.

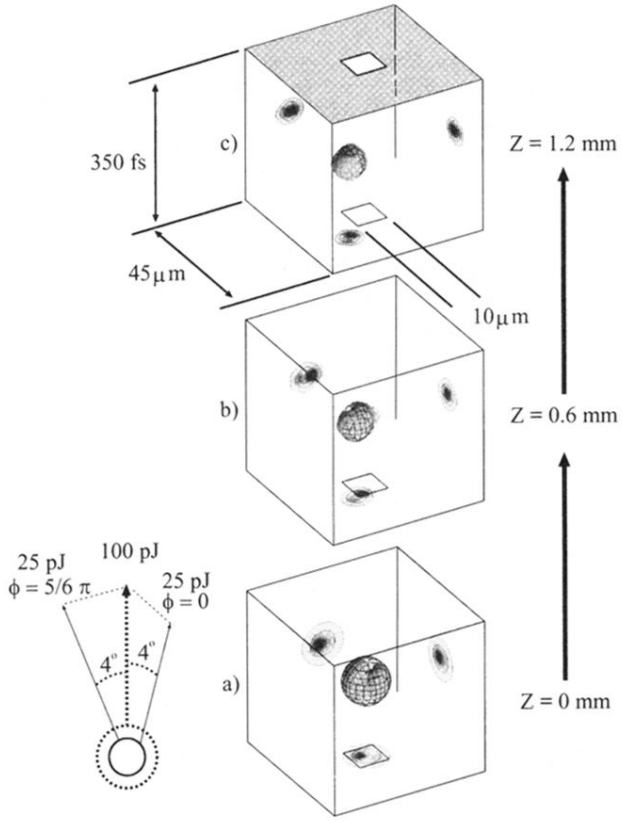

FIG. 12. Simulation of a single-stage NOR gate with a fan in of 2. The signals, in the same polarization, are 5/6 π out of phase and produce an initial interference null. Some energy is radiated, but the majority forms a complex, bound vector soliton which propagates out along the diagonal between $\hat{x}$ and $\hat{y}$.

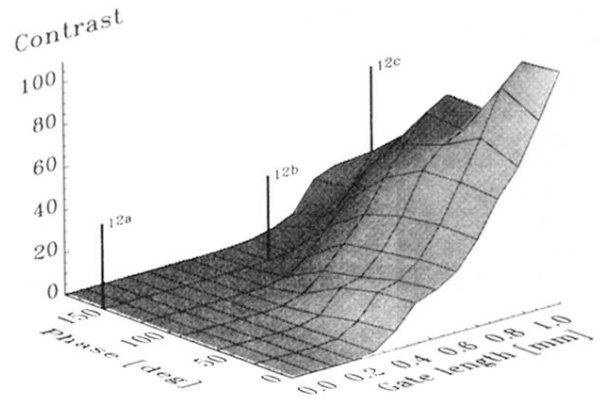

FIG. 13. Contrast of two-input single-stage NOR as a function of gate length and relative phase of the two signals. The labels show the positions of the frames rendered in the preceding figure.

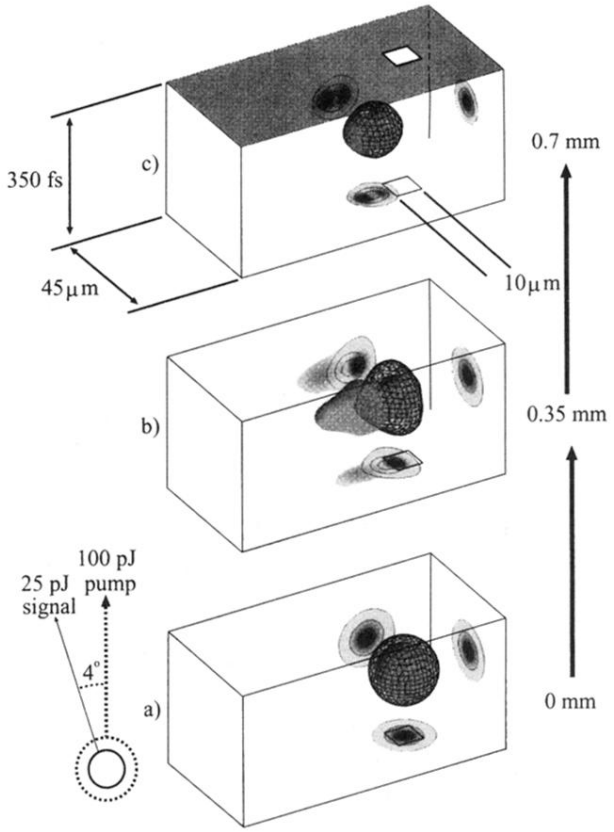

FIG. 9. Light-bullet dragging with a gain of 4 resulting in a contrast of 32 in 880 μm. The three frames shown the 100 pJ pump light bullet, rendered as a grid isosurface at 1/10 its total intensity, interacting with the 25 pJ signal light bullet, rendered as a solid isosurface at the same intensity. The energy of both the pump and the signal are projected onto the three back faces of the box and rendered as contour plots (with contours at -3, -10, and -20 dB of peak) and density maps, respectively. The position of the 10 μm square aperture is indicated and can be used (by comparison with the projected pump intensity contours) to estimate the success of the dragging operation.